EUROPEAN HEMATOLOGY ASSOCIATION
haematologica
Journal of the European Hematology Association

Macrophage ferroportin is essential for stromal cell proliferation in wound healing

by Stefania Recalcati, Elena Gammella, Paolo Buratti, Andrea Doni, Achille Anselmo, Massimo Locati, and Gaetano Cairo

Haematologica 2018 [Epub ahead of print]

Citation: Stefania Recalcati, Elena Gammella, Paolo Buratti, Andrea Doni, Achille Anselmo, Massimo Locati, and Gaetano Cairo. Macrophage ferroportin is essential for stromal cell proliferation in wound healing. Haematologica. 2018; 103:xxx
doi:10.3324/haematol.2018.197517

Macrophage ferroportin is essential for stromal cell proliferation in wound healing

Stefania Recalcati [1#], Elena Gammella [1#], Paolo Buratti [1], Andrea Doni [2], Achille Anselmo [2], Massimo Locati [2,3*], Gaetano Cairo[1*]

[1] Department of Biomedical Sciences for Health, University of Milan, Italy;

[2] Humanitas Clinical and Research Center, Rozzano, Italy;

[3] Department of Medical Biotechnologies and Translational Medicine, University of Milan, Italy.

# SR and EG contributed equally to this work

Running head: stromal cells need macrophage iron

[*] **Corresponding authors:**

Gaetano Cairo (gaetano.cairo@unimi.it); Department of Biomedical Sciences for Health, University of Milan, Italy.

Massimo Locati (massimo.locati@humanitasresearch.it or massimo.locati@unimi.it); Department of Medical Biotechnologies and Translational Medicine, University of Milan, Italy; Humanitas Clinical and Research Center, Rozzano, Italy.

Word count: abstract 177 words, main text 4205 words. 6 figures are present in the manuscript. One supplemental file is associated with the manuscript.

ACKNOWLEDGEMENTS

This work was supported by grants from the Italian Association for Cancer Research (AIRC-IG 2016 #19213 to ML) and MIUR (COFIN to GC). The authors would like to thank Nancy Andrews for providing $Fpn^{fl/fl}$ mice, Alberto Mantovani for support and helpful comments, Eugenio Scanziani and Camilla Recordati for help with histological analysis.

ABSTRACT

Iron recycling by macrophages is essential for erythropoiesis, but may be also relevant for iron redistribution to neighbouring cells at the local tissue level. Using mice with iron retention in macrophages due to targeted inactivation of the iron exporter ferroportin, we investigated the role of macrophage iron release in hair follicle cycling and wound healing, a complex process leading to major clinical problems, if impaired. Genetic deletion of ferroportin in macrophages resulted in iron deficiency and decreased proliferation in epithelial cells, which consequently impaired hair follicle growth and caused transient alopecia. Hair loss was not related to systemic iron deficiency or anemia, thus indicating the necessity of local iron release from macrophages. Inactivation of macrophage ferroportin also led to delayed skin wound healing with defective granulation tissue formation and diminished fibroplasia. Iron retention in macrophages had no impact on the inflammatory processes accompanying wound healing, but affected stromal cells proliferation, blood and lymphatic vessels formation, and fibrogenesis. Our findings reveal that iron/ferroportin plays a largely underestimated role in the macrophage trophic function in skin homeostasis and repair.

INTRODUCTION

Tissue resident macrophages play an important role both in tissue homeostasis, by supporting neighboring parenchymal cells with trophic signals and nutrients, and in tissue repair following injury (1-4). In the skin context, macrophages are critical regulators of hair follicle growth (5) and cutaneous wound healing, two events with many similarities (6). Indeed, perifollicular macrophages prompt the entry of hair follicle stem cells in the anagen phase of growth (7), while selective ablation of macrophages impaired the wound healing response (8). Although wound macrophages display a mixed phenotypic and functional profile, the initial phase is characterized by the prevalence of pro-inflammatory classically activated M1 macrophages, which are associated with the production of oxygen radicals and pro-inflammatory cytokines. Conversely, at later stages during inflammation resolution and tissue repair, alternatively polarized M2 macrophages oriented to tissue repair and remodeling, predominate (1, 9). This M1 to M2 switch is required for normal healing (2).

Macrophages also are at the cross road of iron traffic (10, 11). Iron-recycling macrophages provide iron for erythropoiesis by clearing senescent erythrocytes (12). Conversely, iron sequestration by pro-inflammatory macrophages is a well-known efficient bacteriostatic mechanism in host defense (13). In line with their different functions in homeostatic and inflammatory conditions, polarized macrophages show considerable differences in their transcriptional profile (14), including a distinct regulation of genes related to iron metabolism (11, 15). Iron retention by M1 macrophages correlates with high expression of the iron storage protein ferritin. Conversely, M2 macrophages display increased heme uptake and production of anti-inflammatory mediators via heme oxygenase-dependent heme catabolism, as well as high expression of the iron exporter ferroportin (FPN) (16).

A tight control of iron metabolism is needed for appropriate tissue homeostasis and healing. Excess iron, both in macrophages and in the extracellular milieu, has a deleterious effect on tissue

repair (17), and heme iron has pro-oxidant and pro-inflammatory properties, so that its clearance and degradation by M2 macrophages contributes to resolution (18). However, it is also conceivable that increased iron retention in macrophages leads to lower iron availability for neighbouring cells, thus compromising the trophic role of macrophages. In fact, given the necessity of iron for many essential biological functions, including cell replication (19, 20), defective iron release can jeopardize iron-dependent functions essential for cutaneous homeostasis and efficient tissue restoration. Decreased iron availability could impair the growth of fibroblasts, epithelial and endothelial cells during new tissue formation. Moreover, the hydroxylases necessary for efficient collagen assembly during the repair phase are iron-dependent enzymes (21).

In this study, we have investigated the role of macrophage iron metabolism in tissue homeostasis and repair exploiting a mouse line with iron retention in macrophages caused by targeted FPN inactivation in cells of the myeloid lineage, thus avoiding artefactual systemic iron overload and other confounding elements, such as increased local iron accumulation in other cell types. Using the skin as a model tissue, we show that macrophage-dependent FPN-mediated iron release is required for hair growth in homeostatic conditions and for efficient wound healing, a process which is essential for survival and also clinically relevant, as nonhealing wounds are a major clinical problem associated with various human diseases (22, 23).

METHODS

Animals.

The crossing of mice carrying a floxed Fpn allele ($Fpn^{fl/fl}$) (24), provided by Dr Nancy Andrews, with mice expressing Cre under the control of the LysM promoter in the C57BL/6J background (25) in order to generate mice with specific FPN-macrophage inactivation ($Fpn1^{fl/fl}LysCre^{+/-}$) is described in detail in the Supplements.

Procedures involving animals handling and care were conformed to protocols approved by the Humanitas Clinical and Research Center in compliance with national (DL 116, GU suppl. 40, 18-2-1992; DL 26, GU 4-3-2014) and international law and policies (EEC Council Directive 2010/63/EU, OJ L 276/33, 22–09-2010; National Institutes of Health Guide for the Care and Use of Laboratory Animals, US National Research Council, 2011). The study was approved by the Italian Ministry of Health. All efforts were made to minimize the number of animals used and their suffering.

Statistical analysis.

Results are expressed as the mean ± SEM. Statistical significance between two groups was assessed by unpaired two-tailed Mann-Whitney test or Student's *t* test with Prism software (GraphPad). For comparison of more than two groups, data were analysed using one-way ANOVA.

Full methods are available in the Supplements.

RESULTS

FPN deletion in macrophages causes hair follicle alterations and alopecia.

To generate mice that lack FPN in macrophages, we crossed $Fpn^{fl/fl}$ mice (24) with LysMCre mice (25) to create myeloid cell–specific FPN knockout mice. The phenotypical characterization of these $Fpn1^{fl/fl}LysCre^{+/-}$ mice is described in the Supplements and shown in Fig S1. FPN deletion in macrophages resulted in a significant decrease in hematological parameters [haemoglobin (Hb) levels, hematocrit (Hct) (Fig 1 A and B), red blood cells, MCV and MCH (Table S1)] at weaning (3 weeks after birth). Thereafter, both parameters rapidly returned to normal levels and remained almost unaltered until 18 weeks. In line with the mild anemia observed in 2 month-old 129/SvEvTac mice lacking macrophage FPN (26), in weaned $Fpn1^{fl/fl}LysCre^{+/-}$ mice Hb levels and Hct were lower than in $Fpn1^{fl/fl}LysCre^{-/-}$ at all time-points, though the difference never reached statistical significance (Fig. 1A and 1B). Serum iron levels and transferrin saturation showed a tendency to decrease with age, but were never statistically different between $Fpn1^{fl/fl}LysCre^{+/-}$ mice and their control $Fpn1^{fl/fl}LysCre^{-/-}$ littermates. The hepatic expression of hepcidin (HAMP), which regulates systemic iron homeostasis by inhibiting FPN (20), showed age-related variations but was not different between $Fpn1^{fl/fl}LysCre^{+/-}$ mice and their control littermates. Similarly, we did not detect significant differences in skin HAMP mRNA levels, which were much lower than in the liver (Fig. 1B), while hepcidin levels in skin lysates were undetectable. Accordingly, the expression of Fam132b mRNA encoding for erythroferrone, the erythroid regulator of hepcidin (27), was unchanged in both spleen and bone marrow (Fig. 1B and S2). $Fpn1^{fl/fl}LysCre^{+/-}$ mice showed diffuse alopecia with sparing of the head in 100% of both male and female mice until the fourth week of age (Fig. 1A and 1C). Histological analysis in 3-week-old mice showed no differences between the two genotypes in any organ evaluated, with the exception of the increased iron accumulation in spleen and liver macrophages (Fig. S1) and a moderate/severe and diffuse/multifocal to coalescing dilatation of hair follicles, which contain remnants of hair shafts and keratin, and slight acanthosis

of the superficial epidermis (Fig. 1C). Alopecia gradually disappeared and hair re-growth was evident starting 2 weeks after weaning (Fig. 1A), but minor skin alterations were still detectable in adult Fpn1$^{fl/fl}$LysCre$^{+/-}$ mice, with reduced number of hair follicles, multifocal areas of hair shafts rarefaction and thin hypodermis with an apparent increase of adipose tissue (Fig. 1D). Taken together, these results indicate that targeted FPN deletion in macrophages results in severe alterations of the hair follicle and transient alopecia.

Alopecia is not related to systemic iron deficiency.

In Fpn1$^{fl/fl}$LysCre$^{+/-}$ mice hair regrowth was not complete until 3 weeks after weaning, while Hb levels and Hct were already returned to normal after 1 week (Fig. 1A) and at all time points there was no difference in serum iron availability between Fpn1$^{fl/fl}$LysCre$^{+/-}$ and control littermates. This suggested that alopecia in Fpn1$^{fl/fl}$LysCre$^{+/-}$ mice was not a local reflection of systemic iron deficiency but a consequence of iron sequestration in skin macrophages, ultimately resulting in impaired hair follicle growth. To further assess this issue, we analysed hematologic parameters and alopecia after exposure to low iron diet according to the protocol outlined in Fig. 2A. Until week 5, both Fpn1$^{fl/fl}$LysCre$^{+/-}$ and control littermates were anemic, and Hb levels and other hematologic parameters were always slightly and not significantly lower in animals lacking macrophage FPN (Fig. 2B and 2C, Table S1). Serum iron levels and transferrin saturation were lower in 3-week-old Fpn1$^{fl/fl}$LysCre$^{+/-}$ mice than in control littermates, though not significantly, but returned to normal levels at 6 weeks without differences between the two strains (Fig. 2C). Liver hepcidin expression was repressed by the iron-deficient diet, but was not different between Fpn1$^{fl/fl}$LysCre$^{+/-}$ mice and their control littermates (Fig. 2C). HAMP mRNA levels in the skin were below the detection threshold. A significant increase in erythroferrone expression was found in Fpn1$^{fl/fl}$LysCre$^{+/-}$ pups at 3 weeks (Fig. 2C and S2), indicative of higher erythropoietic activity. After the introduction of the normal diet, both hepcidin and erythroferrone expression returned to normal levels (Fig. 2C and S2). Mice with loss of macrophage FPN were grossly affected by diffuse alopecia of the trunk

throughout the period of exposure to the low iron diet, whereas Fpn1$^{fl/fl}$LysCre$^{-/-}$ mice, despite low serum iron availability, did not develop alopecia (Fig. 2B). Remarkably, alopecia did not appear in Fpn1$^{fl/fl}$LysCre$^{-/-}$ mice even after exposure to the iron deficient diet for 11 weeks. In Fpn1$^{fl/fl}$LysCre$^{+/-}$ mice, after the reintroduction of a normal diet, Hb and serum iron returned to normal levels 2 weeks before the restoration of normally haired skin (Fig. 2B and 2C), thus indicating that alopecia and hypoferremia/anemia are not associated. Histological analysis showed that in Fpn1$^{fl/fl}$LysCre$^{+/-}$ mice challenged with the low iron diet alopecia was associated with severe follicular keratosis with intraluminal accumulation of keratin and distorted hair shafts and subsequent dilation of the hair follicles. Conversely, no relevant histopathological changes were found in the haired skin of the Fpn1$^{fl/fl}$LysCre$^{-/-}$ mice maintained in the same dietary conditions (Fig. 2D). Both in Fpn1$^{fl/fl}$LysCre$^{+/-}$ and Fpn1$^{fl/fl}$LysCre$^{-/-}$ mice maintained under iron deprivation conditions for 5 weeks and subsequently fed a normal diet for 2 weeks, skin histology showed that hair follicles were in the anagen stage, but in Fpn1$^{fl/fl}$LysCre$^{+/-}$ mice hair shafts did not exit the follicular ostia and follicular keratosis/dilation, increased epidermal hyperplasia and dermal inflammation were observed (Fig. 2E).

FPN deletion in macrophages leads to epithelial iron deficiency and decreased proliferation in cutaneous hair follicles.

Since we showed that iron released by macrophages via FPN supports *in vitro* cell proliferation (15), an important role for FPN in skin macrophages could be to mediate the release of sufficient iron for cell multiplication in the microenvironment. Indeed, confocal microscopy revealed a significantly lower expression of the proliferation marker Ki67 in the epithelial cells of the hair bulbs of 3-week-old Fpn1$^{fl/fl}$LysCre$^{+/-}$ mice (Fig. 3). Conversely, in the same cells we found a strong increase of transferrin receptor (TfR1) expression, indicative of cellular iron deprivation (Fig. 3). Notably, F4/80^{+} macrophages, which are abundant in the skin stroma but with no differences in number between Fpn1$^{fl/fl}$LysCre$^{+/-}$ and Fpn1$^{fl/fl}$LysCre$^{-/-}$ mice (Fig. 3), expressed lower levels of

both Ki67 and TfR1 but increased content of both the L and H subunits of the iron storage protein ferritin (Fig. 3 and S3) as compared to epithelial cells. Qualitative analysis also showed that in $Fpn1^{fl/fl}LysCre^{-/-}$ mice ferritin is detectable only in epithelial cells (Figure S3), whereas in $Fpn1^{fl/fl}LysCre^{+/-}$ ferritin expression is particularly strong in $F4/80^{+}$ macrophages. These results suggest that iron retention in resident macrophages, by starving of iron the neighboring hair follicle cells and hence inhibiting their proliferation, has detrimental effects on tissue homeostasis.

FPN deletion in macrophages compromises wound healing.

Resident macrophages support parenchymal cells with trophic signals, particularly under conditions characterized by increased cell proliferation, such as during tissue repair following injury (2). To test the role of macrophage-derived iron in this context, we investigated the wound healing process after incisional skin damage during the entire time course of repair, i.e. the early-inflammatory (2 days post injury [dpi]), middle-proliferative (7 dpi), and late-remodeling phases (12 dpi). We first investigated FPN expression in FACS-sorted macrophages from wounds; in $Fpn1^{fl/fl}LysCre^{-/-}$ mice FPN mRNA levels progressively increased during repair (Fig. 4A), suggesting a predominant role of FPN in the late phases, whereas, as expected, FPN mRNA was always barely detectable in $Fpn1^{fl/fl}LysCre^{+/-}$ mice. The analysis of other iron-related genes showed a rise in the expression of TfR1, which mediates iron uptake, and a decrease of ferritin H subunit during the middle-late phase of repair in macrophages of $Fpn1^{fl/fl}LysCre^{-/-}$ mice, but not $Fpn1^{fl/fl}LysCre^{+/-}$ mice, evidence of iron deposition in these cells (Fig. 4A). Accordingly, histological analysis showed iron accumulation in wound macrophages of $Fpn1^{fl/fl}LysCre^{+/-}$ mice (Fig. 4B). Hepcidin-dependent FPN modulation should not play a role in wound healing, as liver HAMP expression showed no differences between $Fpn1^{fl/fl}LysCre^{-/-}$ and $Fpn1^{fl/fl}LysCre^{+/-}$ mice during wound repair (Fig. S4A) and HAMP expression in FACS-sorted macrophages was undetectable. Hepcidin levels in the wound lysate, which were much lower than in serum, were not different between $Fpn1^{fl/fl}LysCre^{-/-}$ and $Fpn1^{fl/fl}LysCre^{+/-}$ mice (Fig S4B). Macroscopical analysis of wound size showed that in $Fpn1^{fl/fl}LysCre^{+/-}$ mice the process

of closure was considerably delayed as compared to control littermates, with significantly wider lesions at all time points and a lag of 3-5 days at 3 dpi through 12 dpi (Fig. 4C). Histological analysis performed according to the criteria described in Table S2 supported this observation, as $Fpn1^{fl/fl}LysCre^{+/-}$ mice displayed a more prolonged inflammatory response and delayed granulation tissue formation, associated with diminished fibroplasia, whereas mononuclear cells and granulocytes were unchanged (Fig. 4D).

FPN deletion in macrophages has no impact on leukocyte recruitment and activation in the wound.

Given the role of leukocytes in tissue repair (23), we evaluated leukocyte recruitment in our experimental setting. Neutrophils ($Ly6G^+$ cells) and eosinophils ($CCR3^+$ cells) were abundant at 2 and 7 dpi and decreased thereafter, whereas an inverse trend was evident for T cells ($CD3^+$ cells) and macrophages ($F4/80^+$ cells), which increased at 12 dpi (Fig. 5A). The accumulation kinetics of these cells, which are typical of skin wound healing (22), were not affected by the presence or absence of FPN in macrophages.

Macrophages with different functional orientation have specific roles in the overlapping phases of wound repair (1, 9). As iron accumulation in macrophages might favor the expression of inflammatory mediators (17, 26, 28, 29), we evaluated the levels of inflammatory cytokines in wound lysates, but we did not detect significant differences between the two mouse lines at any time point. Since iron accumulation in macrophages of $Fpn1^{fl/fl}LysCre^{+/-}$ mice could affect their polarization during the healing process (15), we investigated the distribution of the different polarized macrophages. As expected, an increase in $MHCII^+/CD206^-$ M1 macrophages was detected already in the middle-proliferative phase, while a significant increase in $MHCII^-/CD206^+$ M2 macrophages was evident only in the late-remodeling phase, but no difference was found between $Fpn1^{fl/fl}LysCre^{+/-}$ mice and their control littermates (Fig. 5A). Moreover, we evaluated the expression of polarization markers in BMDM exposed in vitro to polarization stimuli, but again no difference was observed for both M1 (iNOS and TNFα) and M2 (Arg1 and YM1) markers (Fig.

5B). The expression of iron-related genes in bone marrow derivided macrophages (BMDM) of $Fpn1^{fl/fl}LysCre^{-/-}$ mice mirrored the pattern previously observed in human polarized macrophages (15), with elevated expression of FPN, TfR1 and the hemoglobin/haptoglobin complex receptor CD163 in M2 macrophages. This finding is in line with the prominent expression of FPN in macrophages of the late phase of repair, when the M2 cells infiltrate is increased (Fig. 4A and 5A). Deletion of macrophage FPN resulted in lower expression of TfR1 and CD163 transcript levels in M2 macrophages (Fig. 5B), possibly as a consequence of iron accumulation.

FPN deletion in macrophages affects stromal cells during wound healing.

Since FPN deletion in macrophages significantly affected the wound healing process but iron accumulation in FPN-deficient macrophages did not alter the inflammatory processes associated with wound healing, we evaluated whether the defective iron release by FPN-deficient macrophages affected the biology of surrounding stromal cells in the wound tissue. Confocal analysis at 7 dpi showed reduced expression in $Fpn1^{fl/fl}LysCre^{+/-}$ mice, as compared to control littermates, of blood (CD31) and lymph vessel (Lyve-1) endothelium markers (Fig. 6). This was accompanied by decreased expression of PDGFRα, a marker of mesenchymal cells, and lower levels of collagen I and αSMA, which are markers of activated fibroblasts and myofibroblasts, respectively (Fig. 6). Moreover, in the absence of macrophage FPN, surrounding stromal cells were iron deficient, as indicated by upregulation of TfR1 expression, and proliferated less than control counterparts, as shown by decreased Ki67 expression (Fig. 6). Taken together, these results indicate that the iron retention in macrophages caused by FPN deletion impairs blood vessels formation and stromal cells proliferation, leading to delayed skin repair.

DISCUSSION

The role of erythrophagocytic macrophages as a source of iron for erythropoiesis is well established (16). However, macrophages may be also involved in iron redistribution at a local tissue level, thus impacting neighbouring cells. We previously showed that FPN-mediated iron release from human macrophages supports *in vitro* cell proliferation (15). In the present study, we showed that a steady supply of iron released by macrophage FPN is essential for tissue homeostasis in two conditions, follicular development and wound healing, which share many similarities, including fast cell growth rate (6). Therefore, our study underlines a new iron-related function of macrophages in tissue homeostasis and regeneration, in line with the increasing recognition of their considerable functional polyvalence and trophic role, in addition to established immunological functions (30). We did not address the effect of FPN gene deletion in other myeloid cells affected in the LysM conditional model here adopted as their contribution to iron storage and release is negligible compared to macrophages (11, 13).

Our findings showing impaired hair follicle growth in mice with FPN-deficiency in macrophages are in line with the report of similar hair and skin lesions in mice with altered expression of other proteins of iron metabolism (31-33), though in these other settings the presence of systemic iron deficiency/anemia did not allow to distinguish the relative contribution of circulating iron vs local availability of macrophage-derived iron. We showed that in mice with loss of macrophage FPN alopecia was not related to limited systemic iron availability, as shown by the lack of differences in serum iron availability and the similar hepatic and local hepcidin expression (Fig 1). Evidence that local iron release from macrophages, which are abundant in skin tissue (Fig. 3), is more important than systemic iron levels was also provided by the persistence of alopecia after the return of normal Hb and body iron levels (Fig. 1 and 2), and by the absence of hair loss in hypoferremic and anemic $Fpn1^{fl/fl}LysCre^{-/-}$ mice (Fig. 2), even when fed an iron deficient for long time. In line with the alopecia and delayed entry of the hair follicle into anagen exhibited by mice

overexpressing H ferritin (34), we provide evidence that iron release from macrophages is required to sustain the rapid multiplication of hair follicle cells (Fig. 3). In the absence of macrophage FPN, follicle epithelial cells are iron deficient, as demonstrated by the increased expression of TfR1, and show a lower replication rate, as indicated by reduced Ki67 levels. The discrepancy with the lack of alopecia in a similar model of macrophage specific FPN inactivation reported by Zhang and colleagues (26) could be explained by the different iron content of the standard diet used (157 ppm vs 232, respectively) and by the different genetic background of the mice. Indeed, the role of dietary iron absorption, which is more important in mice than in humans (35), in correcting the alopecia was also indicated by the effect of switching to chow diet at weaning. Alopecia may result from insufficient iron availability caused by decreased local iron release (this study), Matriptase-dependent severe systemic iron deficiency (32, 33); though the role of local FPN was not addressed by these authors, and iron sequestration in ferritin (34). The absence of alopecia in $Fpn1^{fl/fl}LysCre^{-/-}$ mice kept on iron deficient diet for almost 3 months suggests that local iron release may provide iron more directly in a paracrine fashion when circulating iron levels fall. We conclude that the essential role of macrophages in hair follicle cycling (5) is not only related to their production of growth stimulators like Wnt (7), but also to the ability to supply the growing tissue with iron. Macrophages are part of the nurturing niche of stem cells in various tissues (36), including tumors. The results reported here in skin hair follicles raise the possibility that macrophage-dependent iron provision has a more general role in different stem cell niches.

We also report here a similar role for macrophage-derived iron during skin wound healing, a complex tissue repair process consisting of overlapping phases of inflammation and tissue remodeling in which macrophages play a key role (2). The use of mice lacking FPN selectively in cells of the myeloid lineage allowed us to define the role of macrophage iron in wound healing in the absence of the systemic iron overload and large local iron accumulation present in other models (17, 28). In the present setting, the disruption of iron export from local macrophages delayed wound healing, apparently by preventing neighboring mesenchymal and stromal cells to receive the iron

supply needed for growth/differentiation. In line with the higher FPN expression in M2 than in M1 macrophages (15, 37), the lack of macrophage FPN exerts its major effects in the middle-late phase of repair when the M1 to M2 switch occurs. Indeed, in the late stages, normal M2 skin macrophages export iron through enhanced FPN expression, whereas FPN-deficient macrophages accumulate iron with concomitant induction of ferritin and repression of TfR1 (Fig. 4A). The lower fibrosis score (Fig. 4D) and the decreased expression of collagen-1 and αSMA (Fig. 6) show that the stromal component is compromised, as the absence of macrophage FPN resulted in iron deprivation and impaired proliferation of stromal cells (Fig. 6). In this context, fibroblasts may not receive enough iron, which can be among the paracrine factors secreted by M2 macrophages to favor cell multiplication (38). A detrimental effect on collagen synthesis and assembly, which require iron-dependent prolyl hydroxylases (21), or other iron-dependent functions such as dihydroxy-docosahexaenoic acids production (39), may contribute to defective repair.

Our results also show that macrophage iron is essential for the development of the vascular network during tissue healing, as both lymphatic and blood vessels were reduced (Fig. 6). Though decrease of vascular structure caused by macrophage depletion was previously ascribed to the reduced production of VEGF and TGFβ (9), the latter being also involved in extracellular matrix deposition and αSMA expression (40), in our experimental model these growth factors were unchanged (Fig. S5). Similarly, given that Hb levels of adult $Fpn1^{fl/fl}LysCre^{+/-}$ mice were normal, defective oxygenation as a possible factor involved in impaired vascularization can be ruled out. Therefore, our results showing reduced neovessel density, reduced granulation tissue formation and decreased fibrosis in the absence of macrophage iron release, in face of unchanged levels of prominent angiogenic and fibrogenic factors like VEGF and TGFβ, support the relevance of the trophic role of macrophage-derived iron in the wound milieu.

Understanding the role of iron in macrophage production of inflammatory molecules has been hampered by contradictory findings. An increased inflammatory response was found in iron-depleted macrophages (41), but not in equally iron-deficient macrophages from $HFE^{-/-}$ mice (42),

and other studies showed that iron levels positively correlate with the synthesis of pro-inflammatory cytokines (26, 43). In addition, a pro-inflammatory state has been shown in macrophages and macrophage/microglia cells exposed to heme or iron (28, 29) and in hemorrhagic areas within tumors (44). Similarly, decreased iron release from macrophages associated with pro-inflammatory activation and defective M2 polarization, impaired wound healing in chronic venous leg ulcers (17). Conversely, we found that iron retention in macrophages has no impact on leukocyte recruitment and activation as well as macrophage polarization (Fig. 5 and Fig. S5). Moreover, *in vitro* polarized BMDM derived from the two mouse lines did not show differential expression of M1 and M2 markers (Fig. 5B). Therefore, in our model, iron accumulation does not exacerbate the pro-inflammatory phenotype of wound healing-associated macrophages, in keeping with a recent study showing that iron did not increase M1 polarization of RAW264.7 macrophages (45). These conflicting results may be related to the different experimental models, the heterogeneity of macrophages and the exposure to different iron sources, such as heme iron which is highly toxic (46). In the absence of FPN, macrophages from $Fpn1^{fl/fl}LysCre^{+/-}$ mice accumulate iron in ferritin, which increases less than 2-fold (Fig. 4A), but iron deposition seems less massive than in conditions like chronic ulcers (17), in which iron content may increase 20-fold (47), or hemolysis (29, 44). In our experimental setting iron accumulation may therefore be insufficient to interfere with the M1/M2 switch and favor a pro-inflammatory status. A recent study demonstrated that FPN-downregulation in macrophages impairs skeletal muscle regeneration after injury (48), but the effect of increased iron accumulation on the inflammatory profile of macrophages was not addressed.

In conclusion, the results of our study indicate that local macrophage FPN, by supplying iron to cells in the microenvironment, impacts on both the physiological context of follicular anagen and the pathophysiological context of wound healing. In its absence, stromal cells are iron deficient and their proliferation is impaired (Fig. 3 and 6). The importance of local iron recycling is underlined by the lack of changes in hepatic and skin hepcidin. A similar requirement for iron provided locally by macrophages has been described for the repair of skeletal muscle cells, in which

iron retention in macrophages, by impairing myoblasts proliferation, results in smaller myofibers (48). Therefore, iron should be added to the list of trophic mediators locally produced by macrophages that stimulate the growth, differentiation and activity of neighboring parenchymal and stromal cells in order to maintain tissue homeostasis or repair.

AUTHORS CONTRIBUTION

S.R. designed and coordinated the project, planned and performed experiments, and co-wrote the manuscript. E.G and P.B. performed mouse breeding, most of the experiments and data analysis. A.D and A.A. performed confocal microscopy and FACS analyses, respectively. M.L. supervised the project, provided advice for experiments, discussed the results and co-wrote the manuscript. G.C. conceived and coordinated the study, interpreted data, and co-wrote the manuscript. All authors discussed the results and commented on the manuscript.

CONFLICT-OF-INTEREST

The authors declare that they have no conflict of interests.

REFERENCES

1. Brancato SK, Albina JE. Wound macrophages as key regulators of repair: origin, phenotype, and function. Am J Pathol. 2011;178(1):19-25.
2. Wynn TA, Vannella KM. Macrophages in Tissue Repair, Regeneration, and Fibrosis. Immunity. 2016;44(3):450-462.
3. Mantovani A, Biswas SK, Galdiero MR, Sica A, Locati M. Macrophage plasticity and polarization in tissue repair and remodelling. J Pathol. 2013;229(2):176-185.
4. Biswas SK, Mantovani A. Orchestration of metabolism by macrophages. Cell Metab. 2012;15(4):432-437.
5. Stenn KS, Paus R. Controls of hair follicle cycling. Physiol Rev. 2001;81(1):449-494.
6. Ansell DM, Kloepper JE, Thomason HA, Paus R, Hardman MJ. Exploring the "hair growth-wound healing connection": anagen phase promotes wound re-epithelialization. J Invest Dermatol. 2011;131(2):518-528.
7. Castellana D, Paus R, Perez-Moreno M. Macrophages contribute to the cyclic activation of adult hair follicle stem cells. PLoS Biol. 2014;12(12):e1002002.
8. Mirza R, DiPietro LA, Koh TJ. Selective and specific macrophage ablation is detrimental to wound healing in mice. Am J Pathol. 2009;175(6):2454-2462.
9. Lucas T, Waisman A, Ranjan R, et al. Differential roles of macrophages in diverse phases of skin repair. J Immunol. 2010;184(7):3964-3977.
10. Recalcati S, Locati M, Cairo G. Systemic and cellular consequences of macrophage control of iron metabolism. Semin Immunol. 2012;24(6):393-398.
11. Cairo G, Recalcati S, Mantovani A, Locati M. Iron trafficking and metabolism in macrophages: contribution to the polarized phenotype. Trends Immunol. 2011;32(6):241-247.
12. Soares MP, Hamza I. Macrophages and Iron Metabolism. Immunity. 2016;44(3):492-504.

13. Ganz T, Nemeth E. Iron homeostasis in host defence and inflammation. Nat Rev Immunol. 2015;15(8):500-510.

14. Martinez FO, Gordon S, Locati M, Mantovani A. Transcriptional profiling of the human monocyte-to-macrophage differentiation and polarization: new molecules and patterns of gene expression. J Immunol. 2006;177(10):7303-7311.

15. Recalcati S, Locati M, Marini A, et al. Differential regulation of iron homeostasis during human macrophage polarized activation. Eur J Immunol. 2010;40(3):824-835.

16. Drakesmith H, Nemeth E, Ganz T. Ironing out Ferroportin. Cell Metab. 2015;22(5):777-787.

17. Sindrilaru A, Peters T, Wieschalka S, et al. An unrestrained proinflammatory M1 macrophage population induced by iron impairs wound healing in humans and mice. J Clin Invest. 2011;121(3):985-997.

18. Lundvig DM, Immenschuh S, Wagener FA. Heme oxygenase, inflammation, and fibrosis: the good, the bad, and the ugly? Front Pharmacol. 2012;3:81.

19. Cairo G, Bernuzzi F, Recalcati S. A precious metal: Iron, an essential nutrient for all cells. Genes Nutr. 2006;1(1):25-39.

20. Muckenthaler MU, Rivella S, Hentze MW, Galy B. A Red Carpet for Iron Metabolism. Cell. 2017;168(3):344-361.

21. Markolovic S, Wilkins SE, Schofield CJ. Protein Hydroxylation Catalyzed by 2-Oxoglutarate-dependent Oxygenases. J Biol Chem. 2015;290(34):20712-20722.

22. Singer AJ, Clark RA. Cutaneous wound healing. N Engl J Med. 1999;341(10):738-746.

23. Gurtner GC, Werner S, Barrandon Y, Longaker MT. Wound repair and regeneration. Nature. 2008;453(7193):314-321.

24. Donovan A, Lima CA, Pinkus JL, et al. The iron exporter ferroportin/Slc40a1 is essential for iron homeostasis. Cell Metab. 2005;1(3):191-200.

25. Clausen BE, Burkhardt C, Reith W, Renkawitz R, Förster I. Conditional gene targeting in macrophages and granulocytes using LysMcre mice. Transgenic Res. 1999;8(4):265-277.

26. Zhang Z, Zhang F, An P, et al. Ferroportin1 deficiency in mouse macrophages impairs iron homeostasis and inflammatory responses. Blood. 2011;118(7):1912-1922.

27. Kautz L, Jung G, Valore EV, Rivella S, Nemeth E, Ganz T. Identification of erythroferrone as an erythroid regulator of iron metabolism. Nat Genet. 2014;46(7):678-684.

28. Kroner A, Greenhalgh AD, Zarruk JG, Passos Dos Santos R, Gaestel M, David S. TNF and increased intracellular iron alter macrophage polarization to a detrimental M1 phenotype in the injured spinal cord. Neuron. 2014;83(5):1098-1116.

29. Vinchi F, Costa da Silva M, Ingoglia G, et al. Hemopexin therapy reverts heme-induced proinflammatory phenotypic switching of macrophages in a mouse model of sickle cell disease. Blood. 2016;127(4):473-486.

30. Wynn TA, Chawla A, Pollard JW. Macrophage biology in development, homeostasis and disease. Nature. 2013;496(7446):445-455.

31. Nicolas G, Bennoun M, Porteu A, et al. Severe iron deficiency anemia in transgenic mice expressing liver hepcidin. Proc Natl Acad Sci U S A. 2002;99(7):4596-4601.

32. Du X, She E, Gelbart T, et al. The serine protease TMPRSS6 is required to sense iron deficiency. Science. 2008;320(5879):1088-1092.

33. Folgueras AR, de Lara FM, Pendas AM, et al. Membrane-bound serine protease matriptase-2 (Tmprss6) is an essential regulator of iron homeostasis. Blood. 2008;112(6):2539-2545.

34. Hasegawa S, Harada K, Morokoshi Y, Tsukamoto S, Furukawa T, Saga T. Growth retardation and hair loss in transgenic mice overexpressing human H-ferritin gene. Transgenic Res. 2013;22(3):651-658.

35. Ganz T. Systemic iron homeostasis. Physiol Rev. 2013;93(4):1721-1741.

36. Kaur S, Raggatt LJ, Batoon L, Hume DA, Levesque JP, Pettit AR. Role of bone marrow macrophages in controlling homeostasis and repair in bone and bone marrow niches. Semin Cell Dev Biol. 2017;61:12-21.

37. Corna G, Campana L, Pignatti E, et al. Polarization dictates iron handling by inflammatory and alternatively activated macrophages. Haematologica. 2010;95(11):1814-1822.

38. Ploeger DT, Hosper NA, Schipper M, Koerts JA, de Rond S, Bank RA. Cell plasticity in wound healing: paracrine factors of M1/ M2 polarized macrophages influence the phenotypical state of dermal fibroblasts. Cell Commun Signal. 2013;11(1):29.

39. Lu Y, Tian H, Hong S. Novel 14,21-dihydroxy-docosahexaenoic acids: structures, formation pathways, and enhancement of wound healing. J Lipid Res. 2010;51(5):923-392.

40. Hinz B. Formation and function of the myofibroblast during tissue repair. J Invest Dermatol. 2007;127(3):526-537.

41. Pagani A, Nai A, Corna G, et al. Low hepcidin accounts for the proinflammatory status associated with iron deficiency. Blood. 2011;118(3):736-746.

42. Roy CN, Custodio AO, de Graaf J, et al. An Hfe-dependent pathway mediates hyposideremia in response to lipopolysaccharide-induced inflammation in mice. Nat Genet. 2004;36(5):481-485.

43. Wang L, Johnson EE, Shi HN, Walker WA, Wessling-Resnick M, Cherayil BJ. Attenuated inflammatory responses in hemochromatosis reveal a role for iron in the regulation of macrophage cytokine translation. J Immunol. 2008;181(4):2723-2731.

44. Costa da Silva M, Breckwoldt MO, Vinchi F, et al. Iron Induces Anti-tumor Activity in Tumor-Associated Macrophages. Front Immunol. 2017;8:1479.

45. Gan ZS, Wang QQ, Li JH, Wang XL, Wang YZ, Du HH. Iron Reduces M1 Macrophage Polarization in RAW264.7 Macrophages Associated with Inhibition of STAT1. Mediators Inflamm. 2017;2017:8570818.

46. Gozzelino R, Jeney V, Soares MP. Mechanisms of cell protection by heme oxygenase-1. Annu Rev Pharmacol Toxicol. 2010;50:323-354.

47. Ackerman Z, Seidenbaum M, Loewenthal E, Rubinow A. Overload of iron in the skin of patients with varicose ulcers. Possible contributing role of iron accumulation in progression of the disease. Arch Dermatol. 1988;124(9):1376-1378.

48. Corna G, Caserta I, Monno A, et al. The Repair of Skeletal Muscle Requires Iron Recycling through Macrophage Ferroportin. J Immunol. 2016;197(5):1914-1925.

FIGURE LEGENDS

Figure 1. Transient alopecia and anemia are present in Fpn1$^{fl/fl}$LysCre$^{+/-}$ mice.

(A) Hemoglobin (Hb) levels and haematocrit (Hct) in 3-6-week (w)-old mice (mean ± SEM of n=50 mice for each group; *** $p < 0.0001$, **$p < 0.001$). The histogram at the bottom shows the percentage of alopecia at different time points (mean ± SEM of n=50 mice for each group *** $p < 0.0001$, **$p < 0.001$ vs Fpn1$^{fl/fl}$LysCre$^{-/-}$). (B) Top: Hb levels, Hct, serum iron and transferrin saturation (TS) in 3, 6, 12, 18-week-old mice (mean ± SEM of n=50 mice for each group; *** $p < 0.0001$, ** $p < 0.001$, * $p < 0.01$). Bottom: hepcidin (HAMP) expression in liver (solid bars) and skin (striped bars) and spleen erythroferrone (Fam132b) mRNA levels of 3, 6, 12, 18-week-old mice. mRNA levels were measured by quantitative RT-PCR and normalized to the housekeeping gene 18S RNA. Data are presented as mean ± SEM of n=10 mice for each group. (C) Representative of appearance of 3-week-old Fpn1$^{fl/fl}$LysCre$^{-/-}$ (left) and Fpn1$^{fl/fl}$LysCre$^{+/-}$ (right) mice and representative histology (dorsal area) of the same mice. Magnification 10X, in the inset 20X. (D) Representative histology of the skin (dorsal area) of adult (12-week-old) mice. Tissue sections were stained with hematoxylin and eosin. Magnification: 10X.

Figure 2. Alopecia in Fpn1$^{fl/fl}$LysCre$^{+/-}$ mice is not related to iron deficiency/anemia.

(A) Schematic overview of the feeding protocol: pups were fed by dams kept on iron-deficient diet for 3 weeks until weaning and then maintained on low iron diet for 2 additional weeks followed by normal diet. (B) Hb levels and Hct in 3-8-week-old mice (mean ± SEM of n=10 mice for each group). The histogram at the bottom shows the degree of alopecia at different time points. *** $p < 0.0001$ vs Fpn1$^{fl/fl}$LysCre$^{-/-}$. (C) Top: Hb levels, Hct, serum iron and transferrin saturation (TS) in 3-18-week-old mice (mean ± SEM of n=10 mice for each group; *** $p < 0.0001$). Bottom: hepcidin (HAMP) and erythroferrone (Fam132b) mRNA levels in liver and spleen, respectively, of 3-18-week-old mice. Expression in 3-week-old mice fed the normal diet is shown in comparison. mRNA

levels were measured by quantitative RT-PCR and normalized to the housekeeping gene 18S RNA. Data are presented as mean ± SEM of n = 10 mice for each group; *** $p < 0.0001$, ** $p < 0.001$. (D) Representative histology of the skin (dorsal area) of 3-week-old $Fpn1^{fl/fl}LysCre^{-/-}$ and $Fpn1^{fl/fl}LysCre^{+/-}$ mice maintained with an iron deficient diet. Magnification 20X. (E) Representative histology of the skin (dorsal region) after 5 weeks of iron deficient diet plus 2 weeks of normal diet. Tissue sections were stained with hematoxylin and eosin. Magnification: 10X; 20X in the insets.

Figure 3. Epithelial iron deficiency and decreased proliferation in cutaneous hair follicles of $Fpn1^{fl/fl}LysCre^{+/-}$ *mice.*

Expression and localization of Ki67, F4/80, transferrin receptor (TfR1) and L ferritin subunit (FtL) in cutaneous tissue of $Fpn1^{fl/fl}LysCre^{-/-}$ and $Fpn1^{fl/fl}LysCre^{+/-}$ mice was assessed by confocal microscopy. Representative confocal microscopy images for merged signals, Ki67, TfR1, F4/80 and FtL are shown. Quantification of confocal images (5-9 field of vision/mouse, 3 mice/group) is also reported. *** $p< 0.0001$ vs $Fpn1^{fl/fl}LysCre^{-/-}$. Arrowheads indicate hair bulbs. Bars: 100 μm. Magnification: 40X.

Figure 4. Skin repair is delayed in $Fpn1^{fl/fl}LysCre^{+/-}$ *mice.*

(A) Macrophages ($CD45^+/CD11b^+/Ly6C^+/F4/80^+$) were sorted by FACS from wounded skin tissue of 8 animals/group at 2, 7 and 12 days post injury (dpi) from $Fpn1^{fl/fl}LysCre^{-/-}$ and $Fpn1^{fl/fl}LysCre^{+/-}$ mice. Ferroportin (FPN), transferrin receptor 1 (TfR1) and H-ferritin (FtH) mRNA expression was assessed by qRT-PCR and normalized to the housekeeping gene 18S RNA. Data are presented as mean ± SEM; * $p< 0.01$, ** $p<0.001$, *** $p < 0.0001$. (B) Representative histology of Perls' Prussian blue iron staining of dorsal skin samples at 12 dpi in $Fpn1^{fl/fl}LysCre^{-/-}$ and $Fpn1^{fl/fl}LysCre^{+/-}$ mice. Magnification 40X. A semi-quantitative evaluation of Perls' iron staining is shown on the right. n= 6 for each group; *** $p < 0.0001$. (C) Kinetic analysis of skin excisional wound areas.

Values represent mean ± SEM of n= 24 for each group; * p< 0.01, **p<0.001 vs $Fpn1^{fl/fl}LysCre^{-/-}$. One representative experiment (n= 6 mice/group) out of 4 is shown. The inset shows representative macroscopic images of $Fpn1^{fl/fl}LysCre^{-/-}$ and $Fpn1^{fl/fl}LysCre^{+/-}$ mice skin wounds at 7 dpi. (D) Histological grading of wounds, based on separate evaluation of distinct features of the wound healing process, at 2, 7, 12 dpi. IGT: Immature granulation tissue, MGT: mature granulation tissue. The semiquantitative score was defined as described in Table S2; n= 12 for each group; *** p < 0.0001, ** p < 0.001 vs $Fpn1^{fl/fl}LysCre^{-/-}$.

Figure 5. Wound-infiltrating leukocytes and macrophage polarization are not altered in $Fpn1^{fl/fl}LysCre^{+/-}$ mice.

(A) Frequencies of neutrophils ($CD11b^{+}/Ly6G^{+}$), eosinophils ($CD11b^{+}/CCR3^{+}$), T lymphocytes ($CD3^{+}$), macrophages ($CD11b^{+}/F4/80^{+}$) on $CD45^{+}$ cells. Frequencies of M1 ($MHCII^{+}/CD206^{-}$) and M2 ($MHCII^{-}/CD206^{+}$) polarized macrophages on total live macrophages. Dots and black lines represent single animals and the mean ± SEM, respectively; n=10 mice for each group; *** p < 0.0001, ** p < 0.001, * p < 0.01). (B) BMDMs from $Fpn1^{fl/fl}LysCre^{-/-}$ and $Fpn1^{fl/fl}LysCre^{+/-}$ mice were polarized to M1 and M2 macrophages and relative iNOS, TNFα, Arg1, YM1, FPN, TfR1 and CD163 mRNA levels were measured by qRT-PCR at 24 hours; results were normalized to the housekeeping gene 18S RNA (mean ± SEM of n=12 mice for each group; *** p < 0.0001, ** p < 0.001, * p < 0.01).

Figure 6. Vessel and stromal cells reduction accompanied by iron deficiency and decreased proliferation in wounds of $Fpn1^{fl/fl}LysCre^{+/-}$ mice.

Expression of CD31, Lyve-1, collagen-1, PDFGR, αSMA, Ki67 and TfR1 after skin wounding at 7 dpi was assessed by confocal microscopy and the positive area expressed as %. Each circle represents analysis from a single confocal image (5-9 field of vision/mouse, 6 mice/group), *** p<

0.0001, ** p< 0.001. Representative confocal microscopy images are shown. Bars: 100 μm. Magnification: 40X.

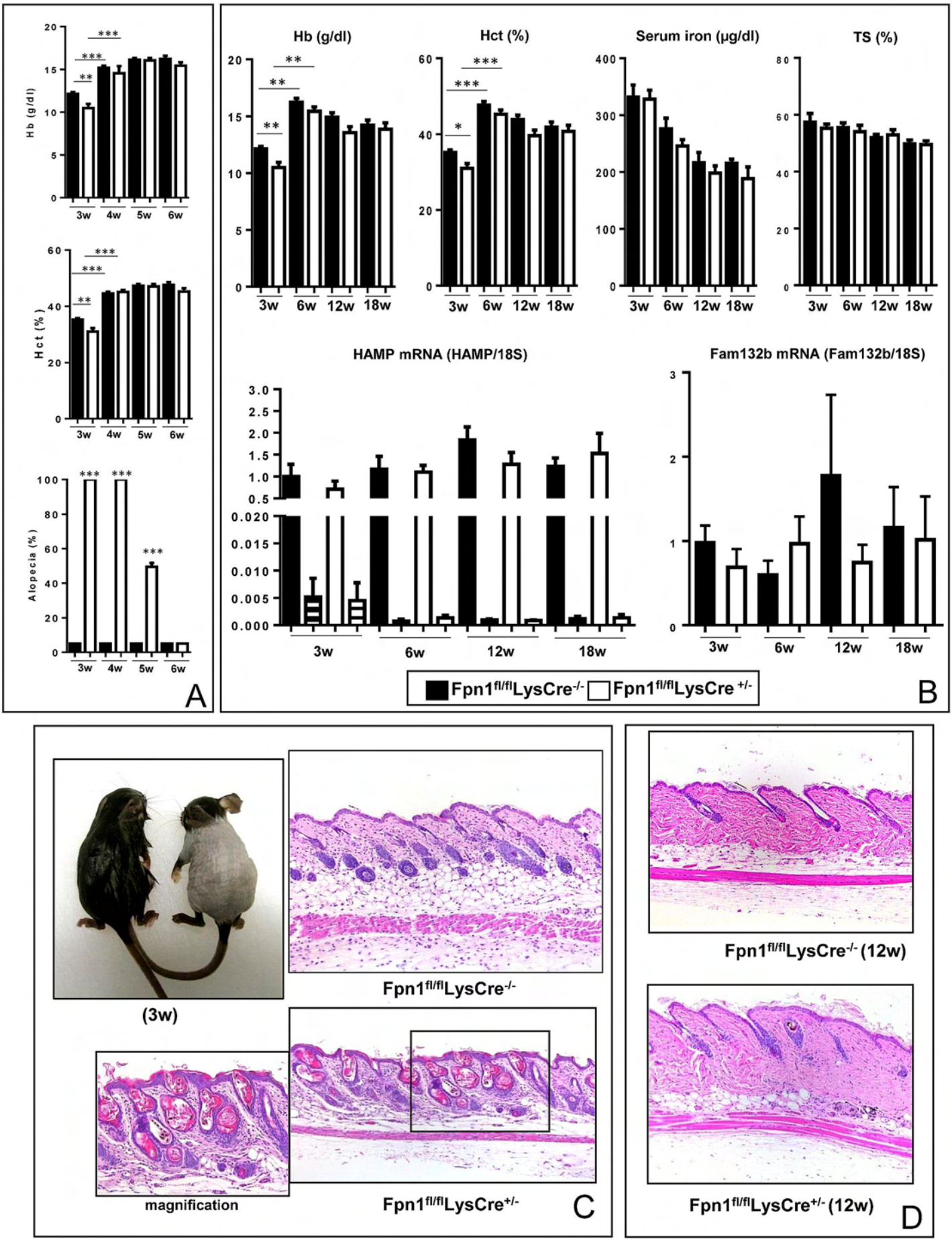
Hb (g/dl)
Hct (%)
Serum iron (μg/dl)
TS (%)
3w 6w 12w 18w
HAMP mRNA (HAMP/18S)
Fam132b mRNA (Fam132b/18S)
Fpn1fl/flLysCre-/- Fpn1fl/flLysCre +/-
A
B
Alopecia (%)
3w 4w 5w 6w
(3w)
Fpn1fl/flLysCre-/-
magnification
Fpn1fl/flLysCre+/-
C
Fpn1fl/flLysCre-/- (12w)
Fpn1fl/flLysCre+/- (12w)
D

Figure 1

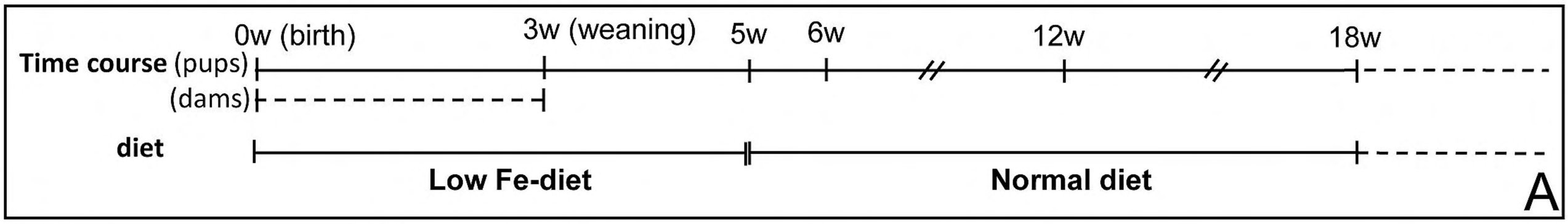
Time course (pups)
(dams)
diet
0w (birth)
3w (weaning)
5w
6w
12w
18w
Low Fe-diet
Normal diet
A

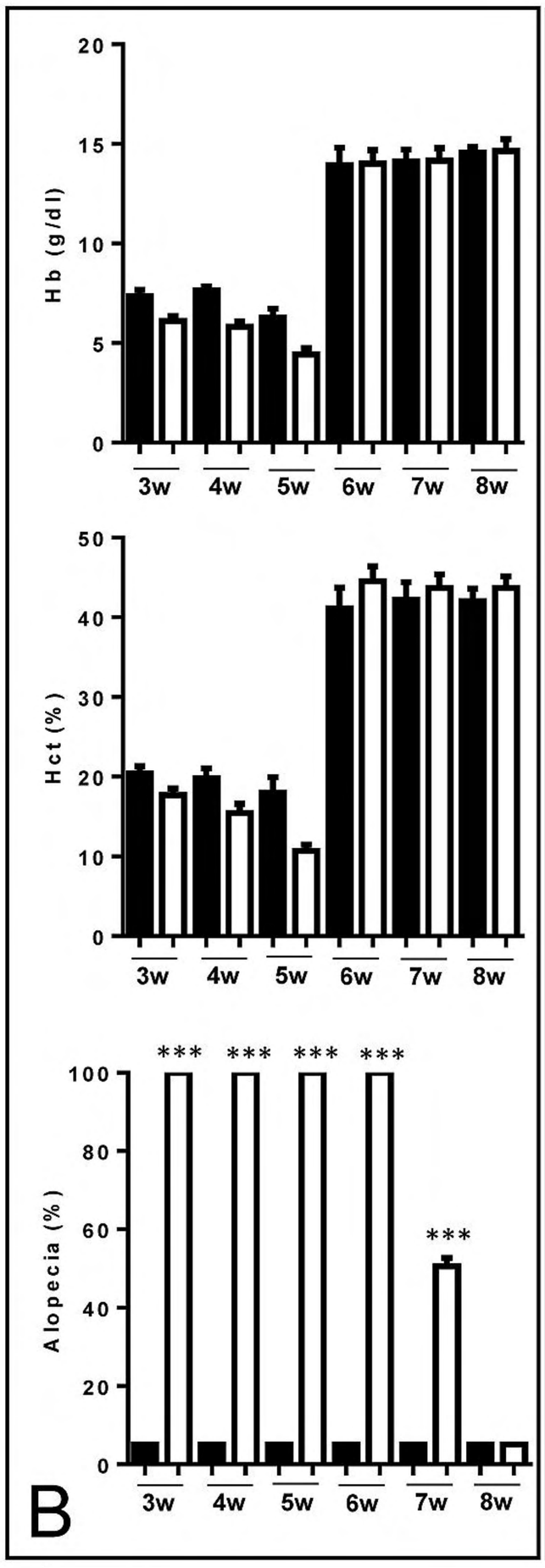
Hb (g/dl)
Hct (%)
3w 4w 5w 6w 7w 8w
*** *** *** ***
Alopecia (%)
B

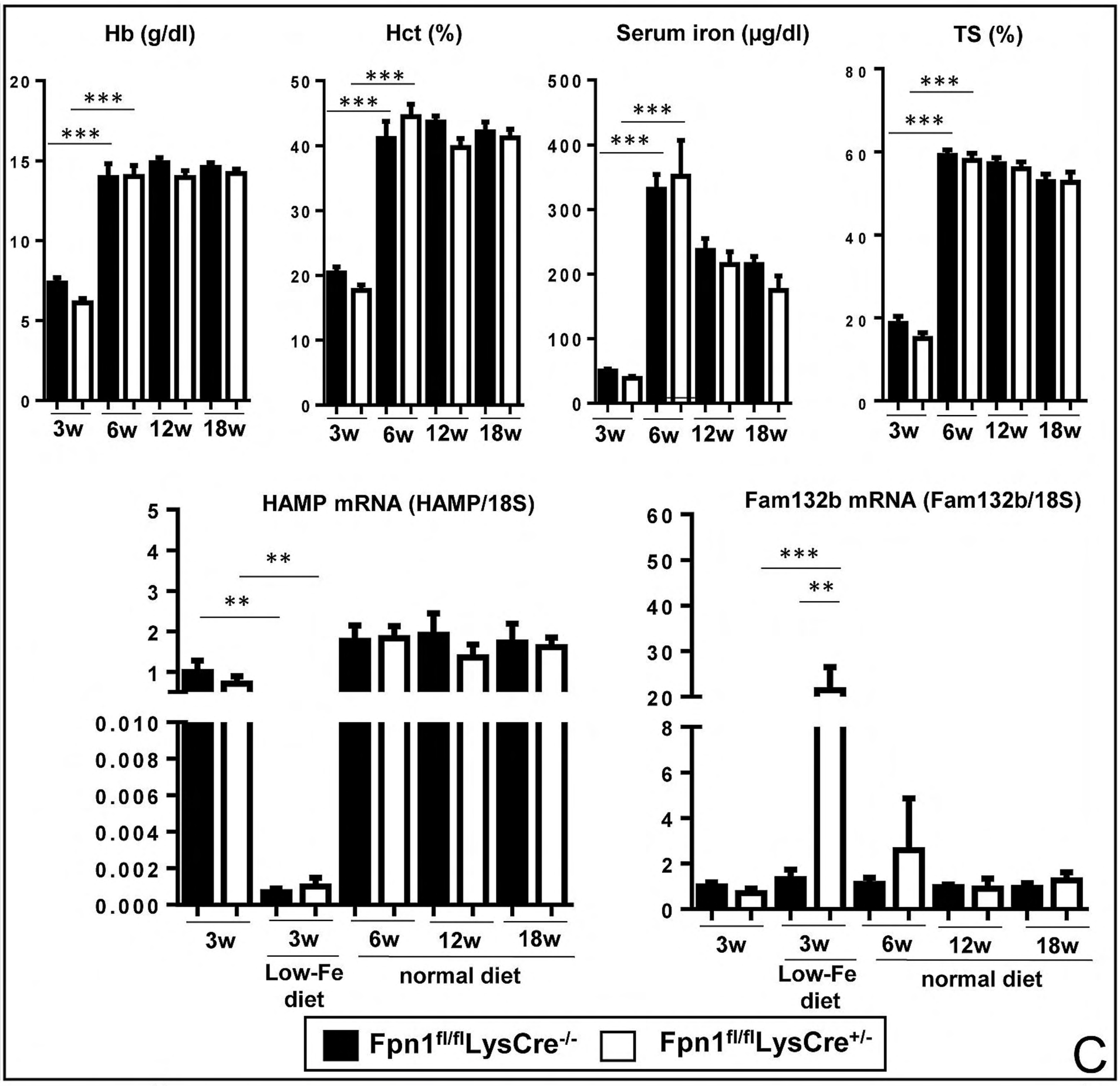
Hb (g/dl)
Hct (%)
Serum iron (µg/dl)
TS (%)
3w 6w 12w 18w
HAMP mRNA (HAMP/18S)
Fam132b mRNA (Fam132b/18S)
Low-Fe diet
normal diet
Fpn1fl/flLysCre-/-
Fpn1fl/flLysCre+/-
C

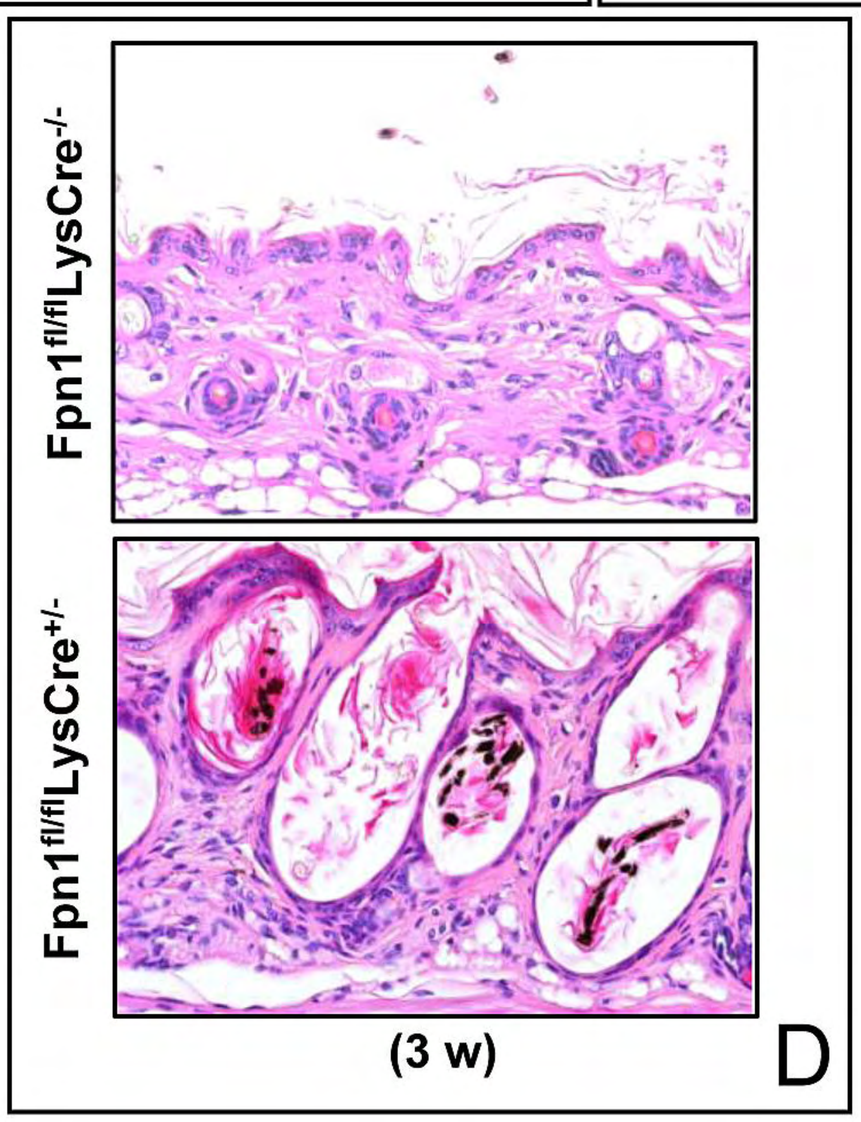
Fpn1fl/flLysCre-/-
Fpn1fl/flLysCre+/-
(3 w)
D

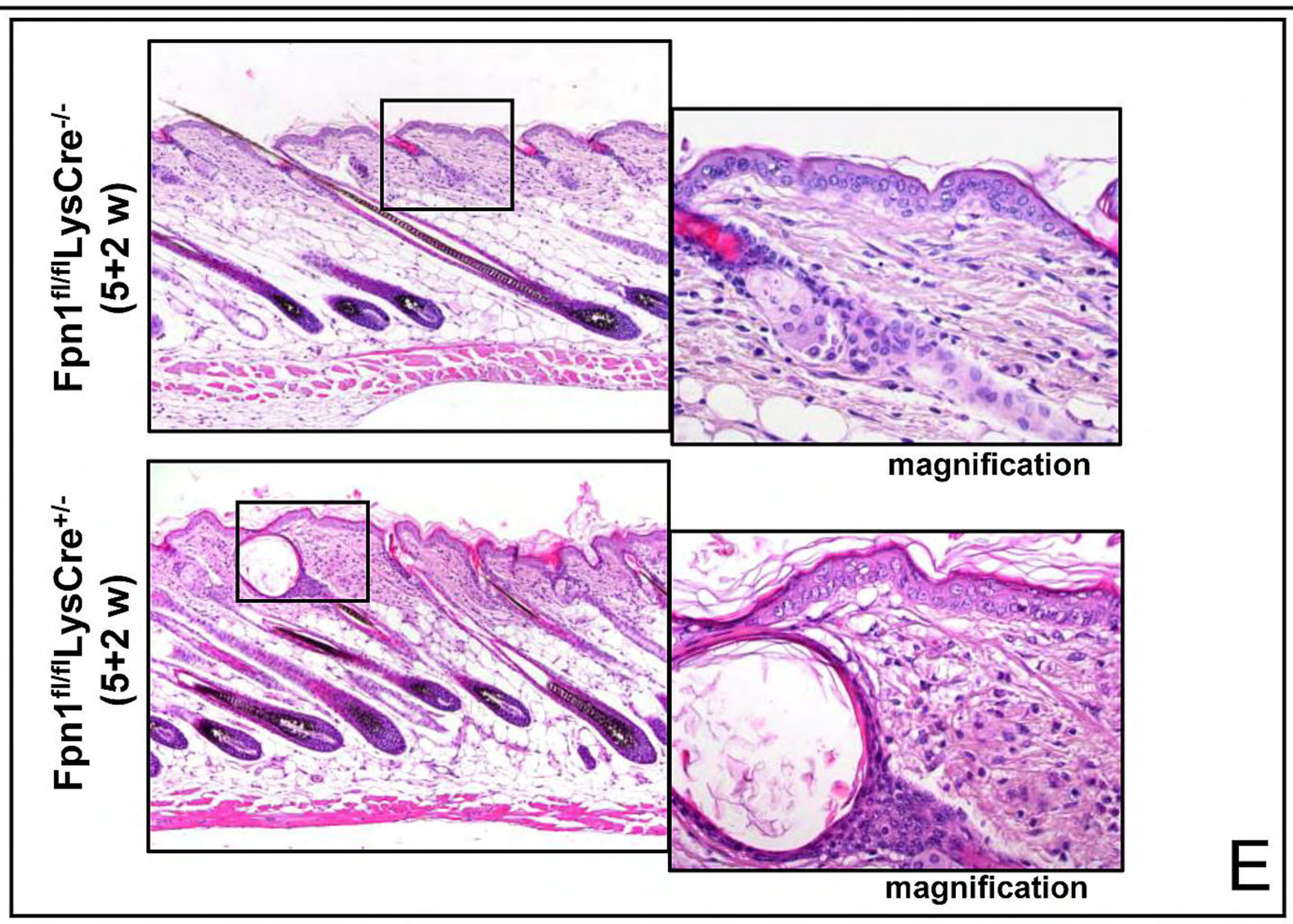
Fpn1fl/flLysCre-/-
(5+2 w)
Fpn1fl/flLysCre+/-
(5+2 w)
magnification
magnification
E

Figure 2

merge
Ki67
F4/80
Fpn1fl/flLysCre-/-
Fpn1fl/flLysCre+/-
merge
TfR1
F4/80
Fpn1fl/flLysCre-/-
Fpn1fl/flLysCre+/-
merge
FtL
F4/80
Fpn1fl/flLysCre-/-
Fpn1fl/flLysCre+/-
Fpn1fl/flLysCre-/-
Fpn1fl/flLysCre+/-
Ki67 positive area
***
F4/80 positive area
TfR1 positive area
***
FtL positive area
***
FtL-F4/80 colocalization rate (%)
***

Figure 3

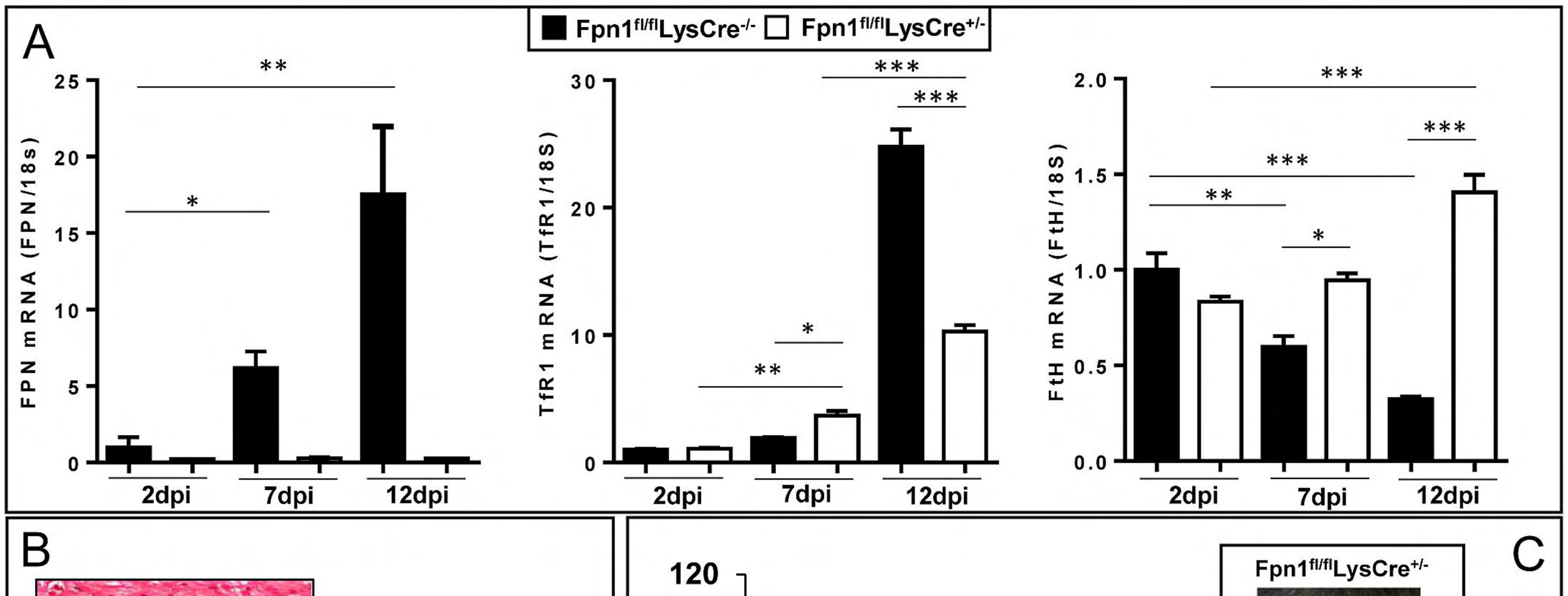
A
Fpn1fl/flLysCre-/-
Fpn1fl/flLysCre+/-
FPN mRNA (FPN/18s)
TfR1 mRNA (TfR1/18S)
FtH mRNA (FtH/18S)
2dpi
7dpi
12dpi

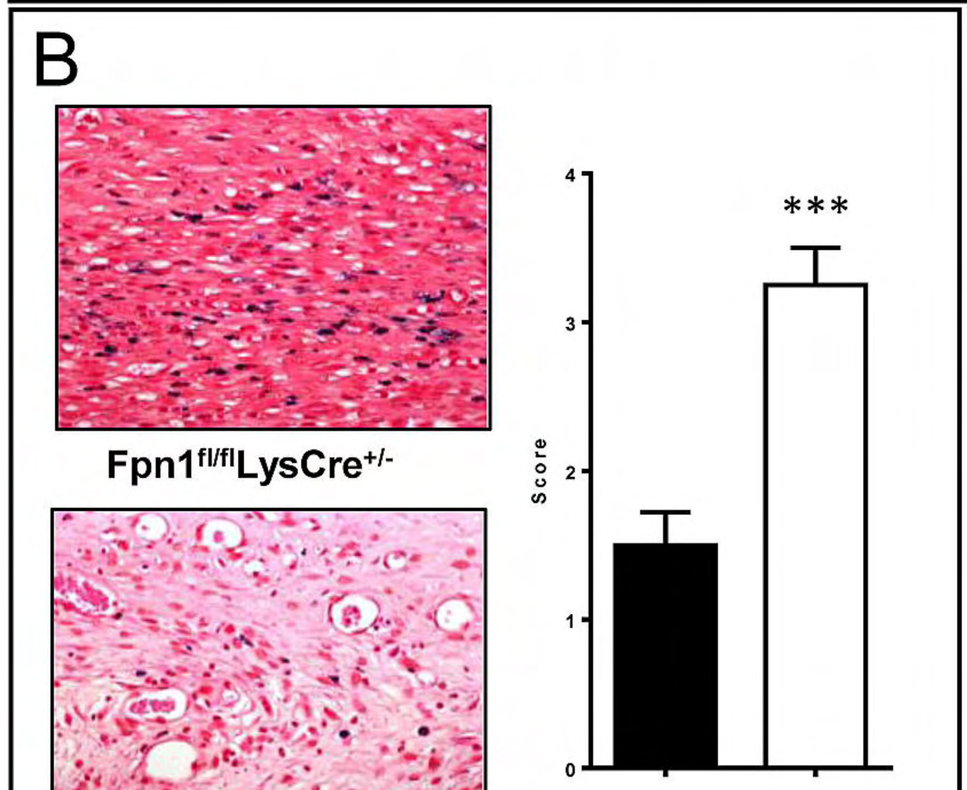
B
Fpn1fl/flLysCre+/-
Fpn1fl/flLysCre-/-
Score
Fpn1fl/flLysCre-/-
Fpn1fl/flLysCre+/-

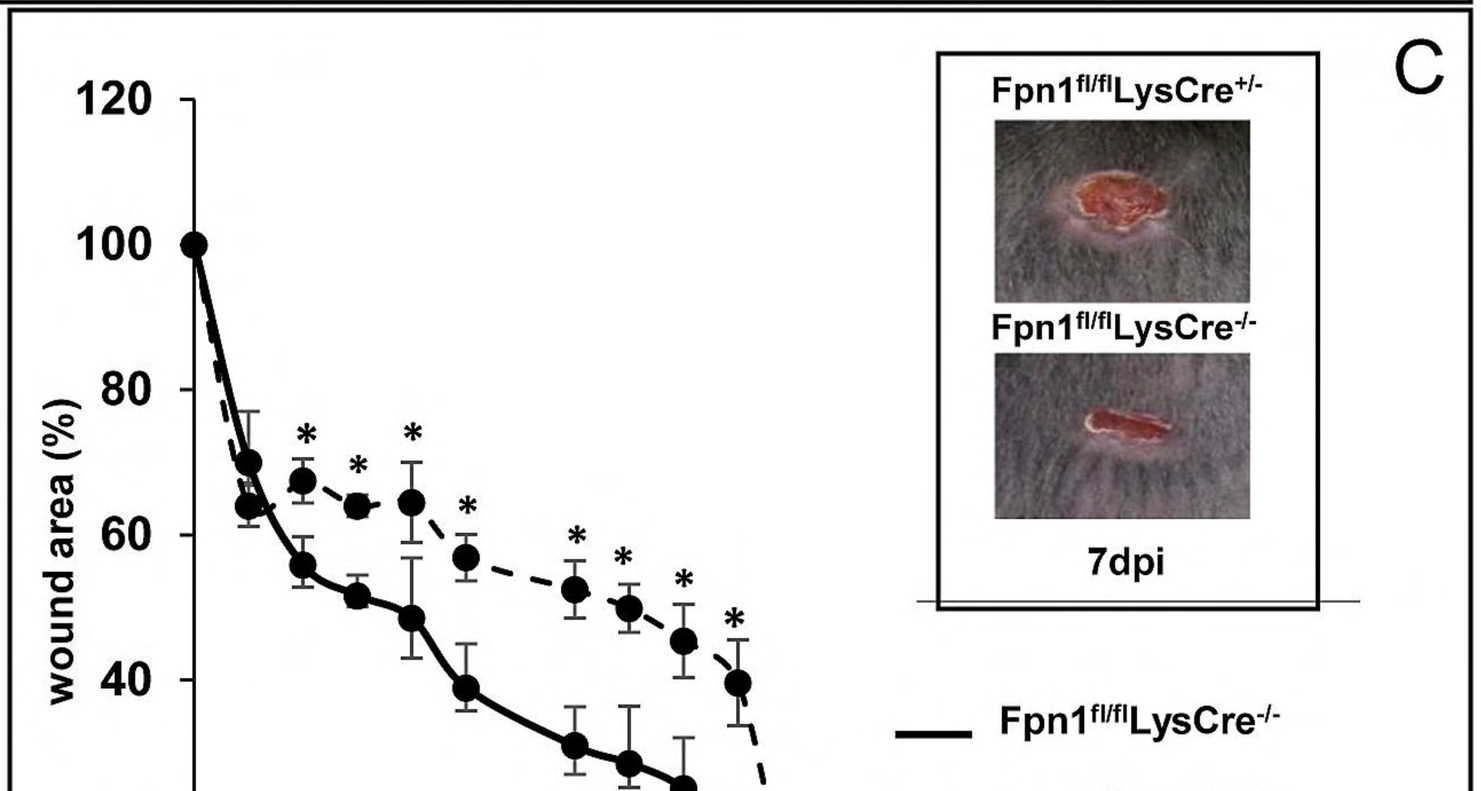
C
Fpn1fl/flLysCre+/-
Fpn1fl/flLysCre-/-
7dpi
wound area (%)
(dpi)
Fpn1fl/flLysCre-/-
Fpn1fl/flLysCre+/-

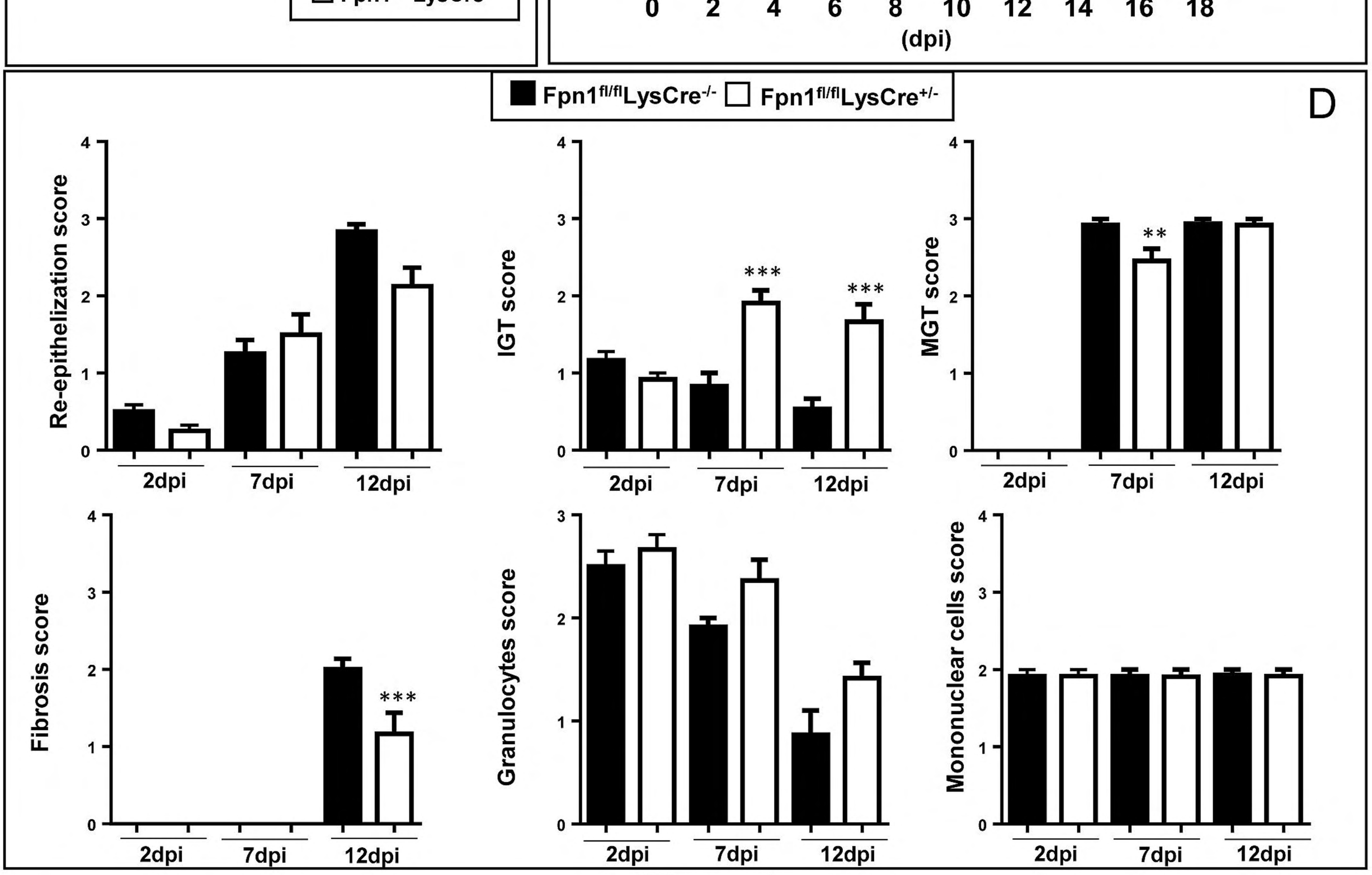
D
Fpn1fl/flLysCre-/-
Fpn1fl/flLysCre+/-
Re-epithelization score
IGT score
MGT score
Fibrosis score
Granulocytes score
Mononuclear cells score
2dpi
7dpi
12dpi

Figure 4

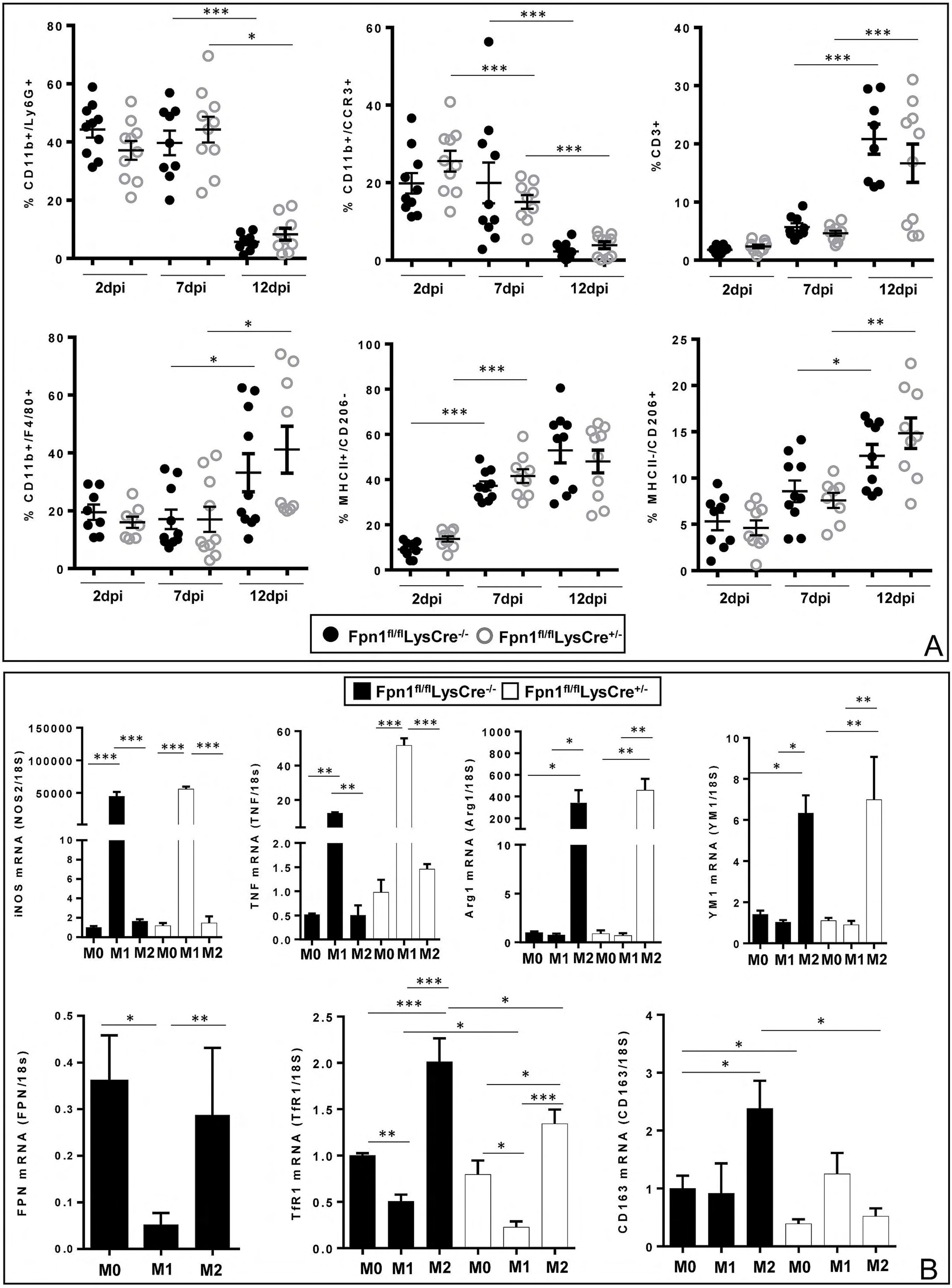
% CD11b+/Ly6G+
% CD11b+/CCR3+
%CD3+
% CD11b+/F4/80+
% MHCII+/CD206-
% MHCII-/CD206+
2dpi
7dpi
12dpi
Fpn1fl/flLysCre-/-
Fpn1fl/flLysCre+/-
A
iNOS mRNA (NOS2/18S)
TNF mRNA (TNF/18s)
Arg1 mRNA (Arg1/18S)
YM1 mRNA (YM1/18S)
M0 M1 M2 M0 M1 M2
FPN mRNA (FPN/18s)
TfR1 mRNA (TfR1/18S)
CD163 mRNA (CD163/18S)
B

Figure 5

Fpn1$^{fl/fl}$LysCre$^{-/-}$ Fpn1$^{fl/fl}$LysCre$^{+/-}$

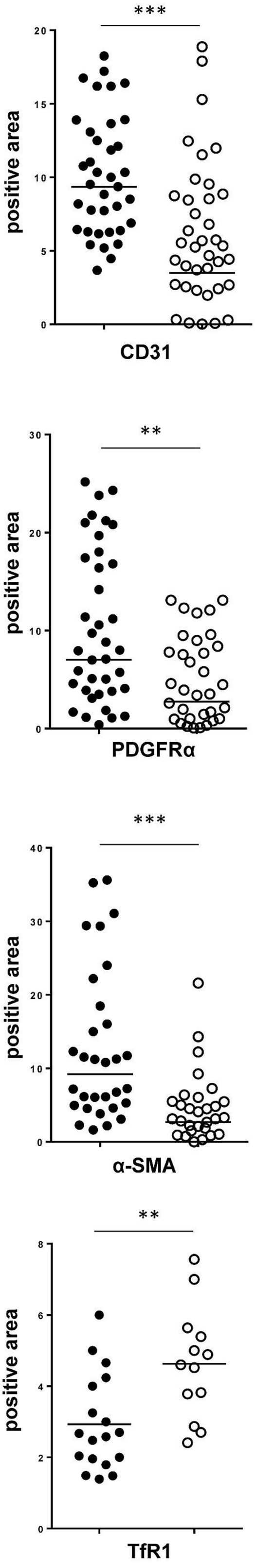

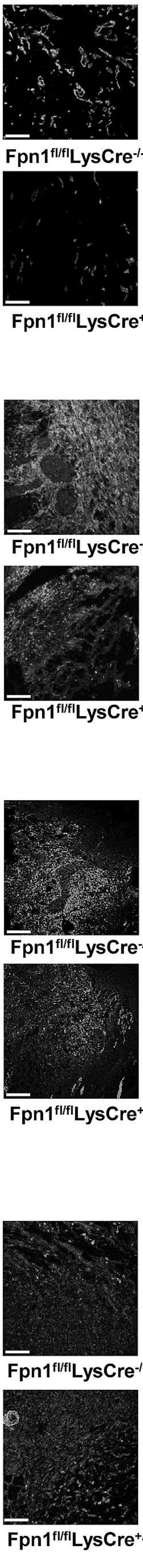

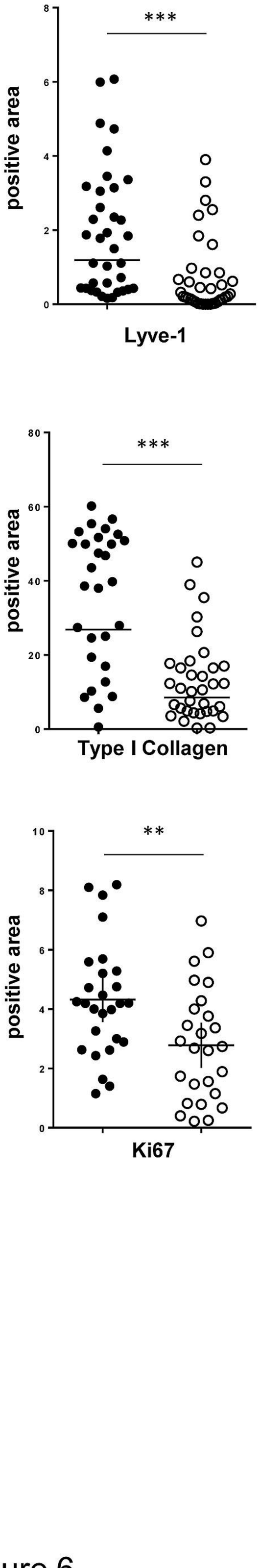

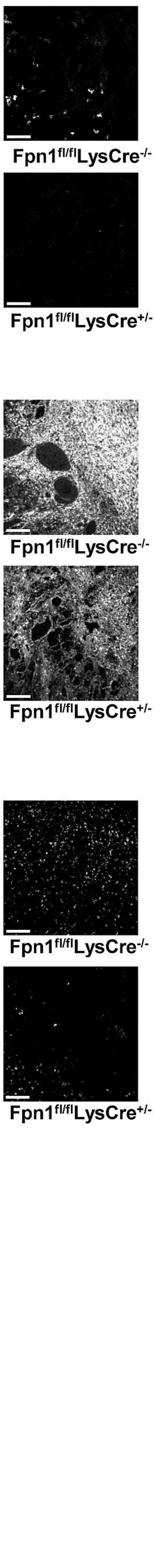

Figure 6

SUPPLEMENTAL METHODS

Animals.

Mice carrying a floxed Fpn allele ($Fpn^{fl/fl}$) (1), generously provided by Dr Nancy Andrews (Duke University), were bred to mice expressing Cre under the control of the LysM promoter in the C57BL/6J background (2) (backcrossed for 11 generations) in order to generate mice with specific FPN-macrophage inactivation ($Fpn1^{fl/fl}LysCre^{+/-}$). $Fpn1^{fl/fl}LysCre^{+/-}$ mice were cohoused with littermates $Fpn1^{fl/fl}LysCre^{-/-}$ mice in individually ventilated cages in a specific pathogen–free animal facility at Humanitas Clinical and Research Center. $Fpn1^{fl/fl}LysCre^{+/-}$ mice were born in mendelian ratios, reproduced normally and did not show significant differences in body weight compared to control floxed littermates ($Fpn1^{fl/fl}LysCre^{-/-}$). Efficient FPN deletion in macrophages was demonstrated in bone marrow derived macrophages (BMDM) and in macrophages derived from peritoneal exudate cells (PEC). Moreover, the functional relevance was shown by the increased iron accumulation revealed in spleen and liver macrophages (Fig. S1). Mice were usually maintained with normal diet (157 ppm iron content). All pups were weaned at 3 weeks of age. When appropriate, dams and pups were provided with an iron-deficient diet (9 ppm iron content; ssniff® EF R/M iron-deficient experimental diet, Charles River). Only some groups were given an iron-deficient diet for 11 weeks after birth, as indicated. Alopecia was quantified as follows: 100% = complete hair loss on the trunk; 50% = initial thin dorsal pelage; 0% = normal coat hair.

Primary cell cultures.

BMDM were generated as previously reported (3). Briefly, bone marrow aspirates from femura of 8- to 12-week old mice were harvested and flushed out with Iscove modified Dulbecco medium (IMDM), 10% fetal calf serum (FCS) (Euroclone, Pero, Italy). After addition of ACK lysis buffer (Thermo Scientific, Milano, Italy) for red cells lysis, bone marrow cells where left to adhere overnight. Non-adherent cells were centrifuged and suspended at 0.5×10^6 cells/mL in complete bone

marrow macrophage medium (IMDM, 10% FCS, 150 μM MTG, 10 ng/mL M-CSF) and cultured for 7 days. BMDM were stimulated by changing the medium to IMDM, 10% FCS, 150 μM MTG, 1% P/S, 1% L-glutamine, and 100 ng/mL LPS plus 20 ng/mL IFNγ or 20 ng/mL IL-4 for 24 h. PEC were recovered from the peritoneal cavity of mice injected with 1 ml of 3% (wt/vol) dithioglycolate (Difco, BD Biosciences, Milano, Italy) as previously reported (4). Briefly, 4-5 days after treatment, peritoneal cells were recovered in 5 ml of saline, centrifuged at 400 x g for 8 minutes, and cultured for 1 h in RPMI. After washing with PBS, adherent macrophages were cultured in RPMI containing 10% FCS.

Immunoblot analysis.

For the preparation of membrane extracts, BMDM and PEC were homogenized in 10 mM Tris-HCl, pH 7.0, 1 mM $MgCl_2$ and the postnuclear supernatant fraction obtained by centrifugation at 2000*g* for 10 minutes was ultracentrifuged at 150000*g* for 20 minutes to pellet crude membrane fractions (5). Equal amounts of protein extracts were electrophoresed in acrylamide-SDS gels, electroblotted to Hybond membranes (Amersham Biosciences, Euroclone) and incubated with antibodies against FPN (1:250; Alpha Diagnostic, DBA, Segrate, Italy). After incubation with the secondary antibody, the protein was detected by means of chemiluminescence (ECL Plus; Amersham Biosciences, Euroclone). Signals were detected using the ChemiDoc Touch system (BioRad, Segrate, Italy) and signal intensity was quantified using ImageLab 5.2.1 software with the values being calculated after normalisation to amido black-stained proteins.

Histology and assessment of tissue sections.

The mice were received as whole body fixed. Organs and tissues were examined for gross lesions, trimmed after complete fixation and processed for paraffin blocks embedding. From each mouse 5 blocks/sections were obtained containing a scheduled list of organs/tissues. For histopathological analysis, 4 μm-thick tissue sections obtained from the paraffin blocks were stained with hematoxylin and eosin. For iron detection, 4 μm sections from each sample were stained with Perls' Prussian blue

stain and semi-quantitatively evaluated under a light microscope as follows: 0 = absence of iron laden cells; 1 = rare iron laden cells; 2 = small number of iron laden cells; 3 = moderate numbers of iron laden cells; 4 = large number of iron laden cells.

Skin wound healing model.

To generate a punch wound, the back of anesthetized mice was shaved and exposed skin was cleaned with 70% ethanol. A full-thickness wound was created with a disposable 8-mm-diam biopsy punch by excising the skin and the underlying *panniculus carnosus* (6). Gentamicin was immediately applied and upon histological analysis no gross infection was apparent through day 14. Wound sites of each mouse were digitally photographed and measured every day in the course of wound healing. The edges of the wounds were daily traced onto a transparency and the areas of open wounds were calculated using ImageJ software (National Institutes of Health). Changes of wound area over time were expressed as percentage of the initial wound areas. The animals were sacrificed at different times and skin biopsies were fixed with 4% paraformaldehyde, and embedded in paraffin or dehydrated with a sucrose gradient and embedded in OCT compound (Diapath, Bergamo, Italy) and stored at -80°C for histology or confocal microscopy analysis, respectively. Alternatively, skin biopsies were directly used for mRNA extraction, FACS and ELISA.

Blood analysis.

Blood was collected by cheek puncture. Hemoglobin, and hematocrit were measured using the Hemo Vet Instrument (Infratec, Portomaggiore, Italy) following manufacturer's instructions; red blood cells, MCV and MHC by using the Sysmex KX-21 automated analyser (Sysmex Italy Cornaredo).

Serum iron determination: blood was collected by cardiac puncture and serum iron was measured using standard laboratory procedures. Transferrin was measured using the mouse transferrin ELISA kit (ab157724, Abcam DBA, Italy) and transferrin saturation was calculated as serum iron concentration (µg/dL) x 100 / [serum transferrin (mg/dL) x 1.42].

ELISA assay.

Whole wounds were collected at 2, 7, and 12 days after wounding and homogenized in 50 mM Tris-HCl, pH 7.5, containing 2 mM EGTA, 1 mM PMSF, 100 KU aprotinin, 1% Triton X-100 (all from Sigma-Aldrich, Milano, Italy), and complete protease inhibitor cocktail (Roche, Monza, Italy). Total proteins were measured by DC Protein Assay, according to manufacturer's instructions (Bio-Rad Laboratories, Segrate, Italy). Cytokine levels were measured in accordance with the manufacturer's instructions (R&D Systems, Space, Milano, Italy). Hepcidin levels were measured using a specific kit (Cloud-Clone Co, Houston, TX, USA) according to the manufacturer's instructions.

Flow cytometry and cell sorting.

A single-cell suspension of wounded skin was generated by cutting samples into small pieces and digestion in PBS (pH 7.4) supplemented with collagenase type I (1 mg/ml; Sigma-Aldrich) and hyaluronidase (125 U/ml; Sigma-Aldrich) at 37°C for 1 h, twice. Finally, a single-cell suspension was obtained by mechanical separation followed by 100 µm filtration and erythrocyte lysis in 0.15 M NH_4Cl, 10 nM $KHCO_3$, 1 nM Na_4EDTA, pH 7.2. The following fluorophore-conjugated antibodies were used for immunophenotyping and intracellular staining: anti–mouse CD45 BV605™ (#30-F11; BD Biosciences); anti–mouse Ly6G PE-CF594™ (#1A8; BD Biosciences); anti–mouse Ly6C BV421™ (#AL-21; BD Biosciences); anti-mouse CD11b PerCP-Cy™5.5 (#M1/70; BD Biosciences); anti-mouse F4/80 PE-Cy7™ (#BM8; BioLegend, Campoverde, Milano, Italy); anti-mouse CD3 APC (#145-2C11 eBioScience, Thermo Fisher); anti mouse MHCII BV711 (#M5/114 BD Biosciences); CD206 PE (#C068C2 BioLegend); CD195 FITC (CCR3) (#J073E5 BioLegend). Dead cells exclusion was performed using LIVE /DEAD fixable Aqua dead cell stain kit (Life Technologies, Thermo Fisher) at room temperature for 15 minutes following the manufacturer instructions. All gated regions were restrictively defined using Fluorescence Minus One as negative control. Stained cells were analysed and/or sorted using FACS LSR Fortessa flow cytometer (BD

Biosciences) or BD FACSAria III cell sorter (BD Biosciences). Diva software (Version 8.0.1) (BD Biosciences) was used for data acquisition and analysis. The purity of sorted cells was ≥ 98%.

Confocal microscopy.

Cryostat sections were incubated in 5% of normal goat (Dako, Milano, Italy) or donkey (Sigma-Aldrich) serum, 2% BSA, 0.1% Triton X-100 (Sigma-Aldrich) in PBS with calcium and magnesium chloride (PBS^{2+}) pH 7.4 for 1 h at room temperature. Specimens were incubated with the following primary antibodies for 2 h at room temperature: rat monoclonal anti-PDGFR (#4C54, 2 µg/ml; Cell Sciences); rabbit polyclonal anti-collagen I (4 µg/ml; AbCam, Euroclone); Cy3-conjugated mouse monoclonal anti-α-SMA (#1A4, 2 µg/ml; Sigma-Aldrich); rabbit monoclonal anti-Ki67 (#D3B5, 1:400; Cell Signaling Technology, Euroclone); rabbit monoclonal anti-TfR1 (0.5 µg/ml; Invitrogen); rat anti-F4/80 (#T45-2342, 1:500, BD Biosciences); rat monoclonal anti-CD31 (#MEC 13.3, 1 µg/ml; BD Biosciences); rabbit polyclonal anti-Lyve-1 (2 µg/ml; AbCam, Euroclone), rabbit polyclonal anti mouse ferritin H subunit (Z17, 1:200) and L subunit (E17, 1:200), both kindly provided by Dr. Maura Poli (University of Brescia, Italy). Sections were then incubated for 1 h with Alexa Fluor® (488, 594, 647)-conjugated species-specific cross-adsorbed detection antibodies (Thermo Fisher Molecular Probes). For DNA detection, DAPI (300 nM; Thermo Fisher-Molecular Probes) was used. After each step, sections were washed with PBS^{2+} pH 7.4 containing 0.01% (vol/vol) Tween 20. Sections were mounted with the antifade medium FluorPreserve Reagent (EMD Millipore, Vimodrone, Italy) and analyzed with an Olympus Fluoview FV1000 laser scanning confocal microscope (Olimpus, Segrate, Italy). Immunoreactive areas were measured using the computer-assisted digital image processing software Image-Pro Plus (version 7.0; Media Cybernetics). The total stained area was automatically selected on the basis of RGB color segmentation and results are expressed as mean percentage of the immunoreactive area ± SEM.

Quantitative real-time polymerase chain reaction (qRT-PCR).

Total RNA isolated from liver, spleen, normal skin, wounds, bone marrow, PEC or BMDM using TRI reagent® (Sigma-Aldrich) was reverse transcribed into cDNA with Proto Script M-MuLV First Strand cDNA Synthesis Kit (New England Biolabs, Euroclone) and the obtained cDNA served as a template for Real-Time PCR, based on the TaqMan methodology (Life Technologies, Thermo Fisher). Thermal cycling parameters were 40 cycle at 95° C for 15s and 60° C for 1 min. Each sample was amplified in triplicate using the primers reported in Table S2 (Applied Biosystems, Thermo Fisher) and the amount of RNA was calculated using the $2^{-\Delta Ct}$ method. Results were normalized to 18S RNA and the housekeeping gene ribosomal protein, large, P0 (RPLPO) with similar results (in the figures only 18S RNA is shown).

SUPPLEMENTAL TABLES

Supplemental Table 1. Haematologic parameters of Fpn1$^{fl/fl}$LysCre$^{-/-}$ and Fpn1$^{fl/fl}$LysCre$^{+/-}$ mice.

	Fpn $^{fl/fl}$LysCre $^{-/-}$		Fpn $^{fl/fl}$LysCre $^{+/-}$		Fpn $^{fl/fl}$LysCre $^{-/-}$		Fpn $^{fl/fl}$LysCre $^{+/-}$	
	3 weeks	6 weeks	3 weeks	6 weeks	3 weeks	6 weeks	3 weeks	6 weeks
	Normal diet				Iron deficient diet			
Red blood cells (x10^6/mm^3)	9.2±0.2	10.4±0.9*	7.7±0.5**	9.8±0.9°°°	6.9±0.4	9.5±0.7***	6.1±0.4	9.4±0.5°°°
MCV (fL)	44±2.6	46±3.5	43±3.1	45±2.1	36±1.9	44.8±3.2***	32.5±1.9	44±2.5°°°
MCH (pg)	14±1.9	15±2.1	13.5±1.9	15±2.9	12.5±0.4	15±0.6***	12±0.4	15±0.7°°°

Data are mean ±SEM, n= 6 for each group. *** p< 0.0001, ** p< 0.001, * p< 0.01 vs 3-week-old Fpn1$^{fl/fl}$LysCre$^{-/-}$ mice; °°° p< 0.0001 vs 3-week-old Fpn1$^{fl/fl}$LysCre$^{+/-}$ mice. MCV indicates mean corpuscular volume, MCH mean corpuscular haemoglobin.

Supplemental Table 2. Wound healing histological grading.

The grading is based on separate evaluation of distinct features of wound healing process.

Response	Cell type	Score			
		0	1	2	3
Re-epithelialization	Migration of epidermal cells from the edges to the center of the wound	Absent	Mild (<50% of the wound)	Moderate (>50% of the wound, but still incomplete)	Complete
Granulation tissue	Immature: loose granulation tissue composed of fibroblasts and macrophages with emerging disorganized vessels	Absent	Wound bed partially covered with granulation tissue	Thin granulation tissue over the whole bed	Thick granulation tissue over the whole bed
	Mature: fibroblasts, initial collagen deposition (loose collagen fibers), perpendicular arranged blood vessels	Absent	Wound bed partially covered with granulation tissue	Thin granulation tissue over the whole bed	Thick granulation tissue over the whole bed
Fibrosis*	More abundant and regular collagen deposition (dense collagen fibers), fewer fibroblast/fibrocytes and vessels	Absent	Mild amount of dense collagen fibers between fibroblast	Moderate amount of dense collagen fibers between fibroblast	Large amount of dense collagen fibers between fibroblast
Inflammation	Mononuclear cells Infiltrate	Absent	Mild	Moderate	Heavy
	Granulocyte infiltrate	Absent	Mild	Moderate	Heavy

* Transition from mature granulation tissue and fibrosis was occurring at late time-point (dpi 12). In this case, the amount of deposition of dense extracellular matrix, i.e. collagen fibers, was evaluated.

Supplemental Table 3. Primers for qRT-PCR.

Gene	TaqMan gene expression assay ID
TfR1	Mm00441941_m1
Fpn	Mm01254820_m1
Rn18s	Mm03928990_g1
FtH	Mm04336019_g1
Fam132b	Mm00557748_m1
Arg1	Mm00475988_m1
TNFα	Mm00443260_g1
iNOS	Mm00440502_m1
Hepcidin	Mm04231240_s1
CD163	Mm00474091_m1
YM1	Mm00657889_mH

REFERENCES

1. Donovan A, Lima CA, Pinkus JL, Pinkus GS, Zon LI, Robine S, et al. The iron exporter ferroportin/Slc40a1 is essential for iron homeostasis. Cell Metab. 2005 Mar;1(3):191-200.
2. Clausen BE, Burkhardt C, Reith W, Renkawitz R, Förster I. Conditional gene targeting in macrophages and granulocytes using LysMcre mice. Transgenic Res. 1999 Aug;8(4):265-77.
3. Weischenfeldt J, Porse B. Bone Marrow-Derived Macrophages (BMM): Isolation and Applications. CSH Protoc. 2008 Dec;2008:pdb.prot5080.
4. Zhang X, Goncalves R, Mosser DM. The isolation and characterization of murine macrophages. Curr Protoc Immunol. 2008 Nov;Chapter 14:Unit 14.1.
5. Delaby C, Pilard N, Gonçalves AS, Beaumont C, Canonne-Hergaux F. Presence of the iron exporter ferroportin at the plasma membrane of macrophages is enhanced by iron loading and down-regulated by hepcidin. Blood. 2005 Dec;106(12):3979-84.
6. Nakayama Y, Kon S, Kurotaki D, Morimoto J, Matsui Y, Uede T. Blockade of interaction of alpha9 integrin with its ligands hinders the formation of granulation in cutaneous wound healing. Lab Invest. 2010 Jun;90(6):881-94.

SUPPLEMENTAL FIGURE

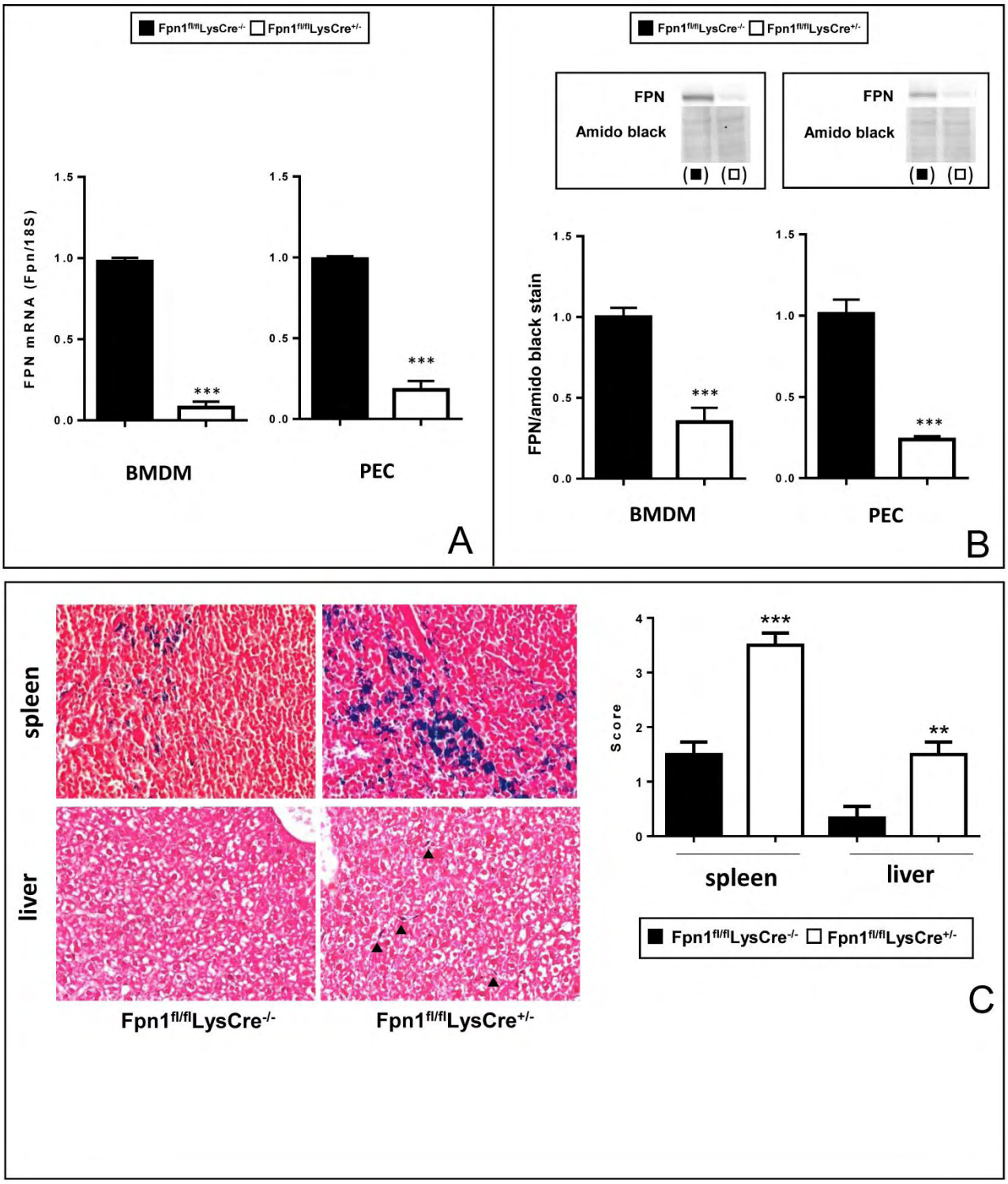

Figure S1. FPN deletion and iron accumulation in macrophages of Fpn1$^{fl/fl}$LysCre$^{+/-}$ mice.

(A) FPN mRNA levels in bone marrow derived macrophages (BMDM) and peritoneal exudate cells (PEC) from Fpn1$^{fl/fl}$LysCre$^{-/-}$ and Fpn1$^{fl/fl}$LysCre$^{+/-}$ mice were measured by quantitative RT-PCR; results were normalized to the housekeeping gene 18S RNA (mean ± SEM of n=50 mice for each group; *** $p < 0.0001$).

(B) Representative blots and densitometric quantitation (mean ± SEM of n=20 mice for each group; *** $p< 0.0001$ vs $Fpn1^{fl/fl}LysCre^{-/-}$) of immunoblot analysis of membrane FPN in BMDM and PEC from $Fpn1^{fl/fl}LysCre^{-/-}$ and $Fpn1^{fl/fl}LysCre^{+/-}$ mice. The blots were stained with amido black to assess equal protein loading. (C) Representative histology of Perls' Prussian blue iron staining in paraffin sections of spleen and liver from $Fpn1^{fl/fl}LysCre^{-/-}$ and $Fpn1^{fl/fl}LysCre^{+/-}$ mice. Arrowheads indicate iron-stained cells in the liver. A semi-quantitative evaluation of Perls' iron staining in spleen and liver (performed as reported in Materials and Methods) is also shown. n = 6 for each group. *** $p< 0.0001$, ** $p< 0.001$ vs $Fpn1^{fl/fl}LysCre^{-/-}$. Magnification: 40X.

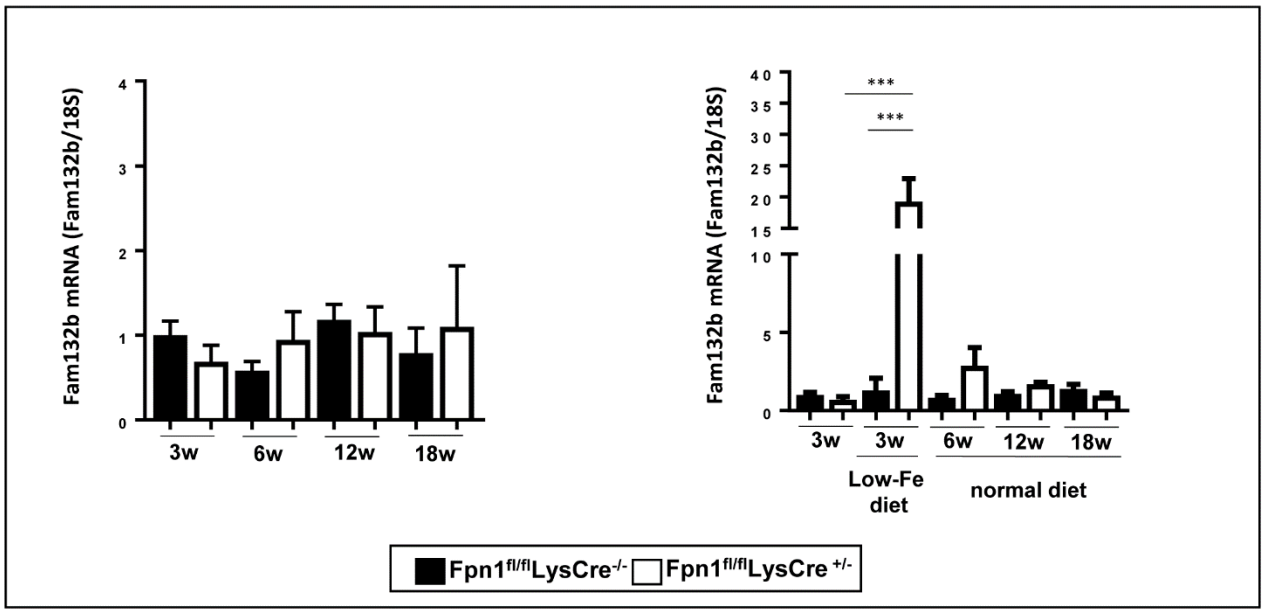

Figure S2. Erythroferrone expression in bone marrow.

Erythroferrone (Fam132b) mRNA levels in the bone marrow of mice fed the normal or the iron-deficient diet at different age. mRNA levels were measured by quantitative RT-PCR and normalized to the housekeeping gene 18S RNA. Data are presented as mean ± SEM. n = 10 mice for each group. *** $p < 0.0001$.

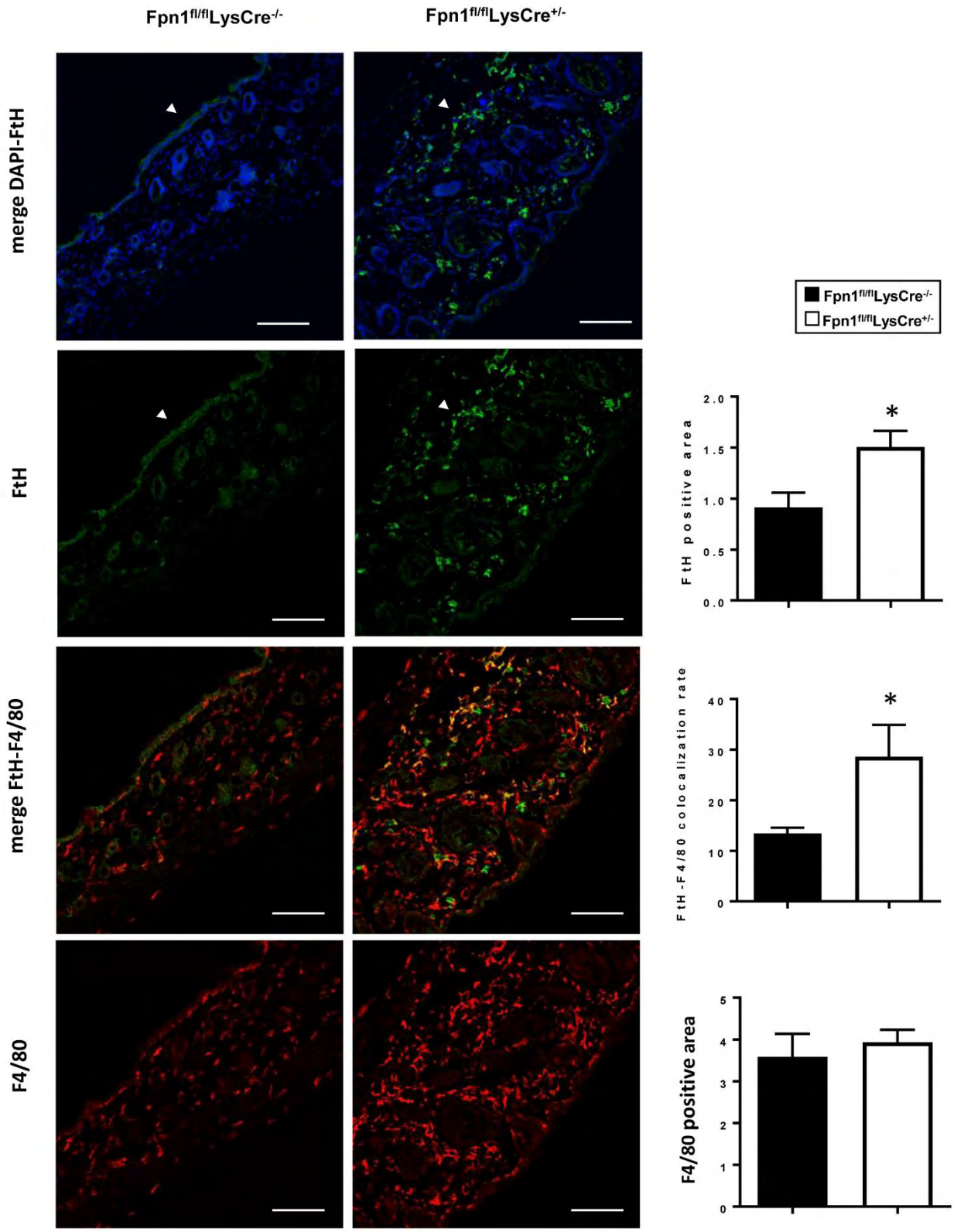

Figure S3. Ferritin expression shows macrophage iron accumulation and epithelial iron deficiency in cutaneous hair follicles of Fpn1$^{fl/fl}$LysCre$^{+/-}$ mice.

Expression and localization of ferritin H subunit (FtH) and F4/80 in cutaneous tissue of Fpn1$^{fl/fl}$LysCre$^{-/-}$ and Fpn1$^{fl/fl}$LysCre$^{+/-}$ mice was assessed by confocal microscopy. Representative confocal microscopy images and

the relative quantification for merge signals, FtH and F4/80 (5-9 field of vision/mouse, 3 mice/group) are shown. * $p < 0.01$ vs $Fpn1^{fl/fl}LysCre^{-/-}$. The top panel shows confocal images of FtH and DAPI counterstain. Arrowheads indicate FtH expression in epithelial cells of $Fpn1^{fl/fl}LysCre^{-/-}$ mice and macrophages of $Fpn1^{fl/fl}LysCre^{+/-}$ mice. Bars: 100 μm. Magnification: 40X.

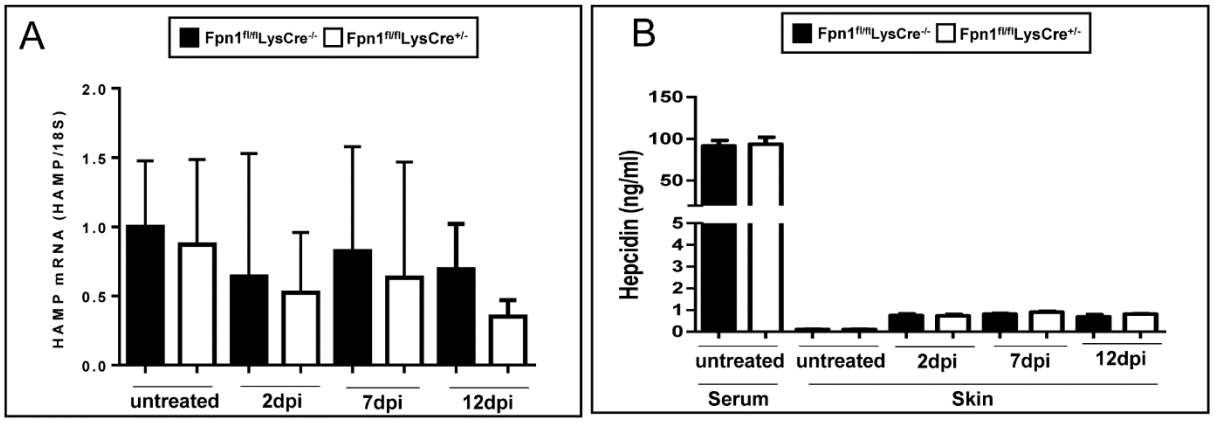

Figure S4. Liver hepcidin expression and hepcidin levels in skin wounds are not altered in Fpn1$^{fl/fl}$LysCre$^{+/-}$ mice.

(A) Hepcidin (HAMP) mRNA levels in liver of mice untreated and at different days post injury (dpi) were measured by quantitative RT-PCR and normalized to the housekeeping gene 18S RNA. Data are presented as mean ± SEM of n=12 mice for each group. (B) Hepcidin protein levels in serum and wound lysates at different dpi were measured by ELISA. n = 4 and 12 for each group, respectively.

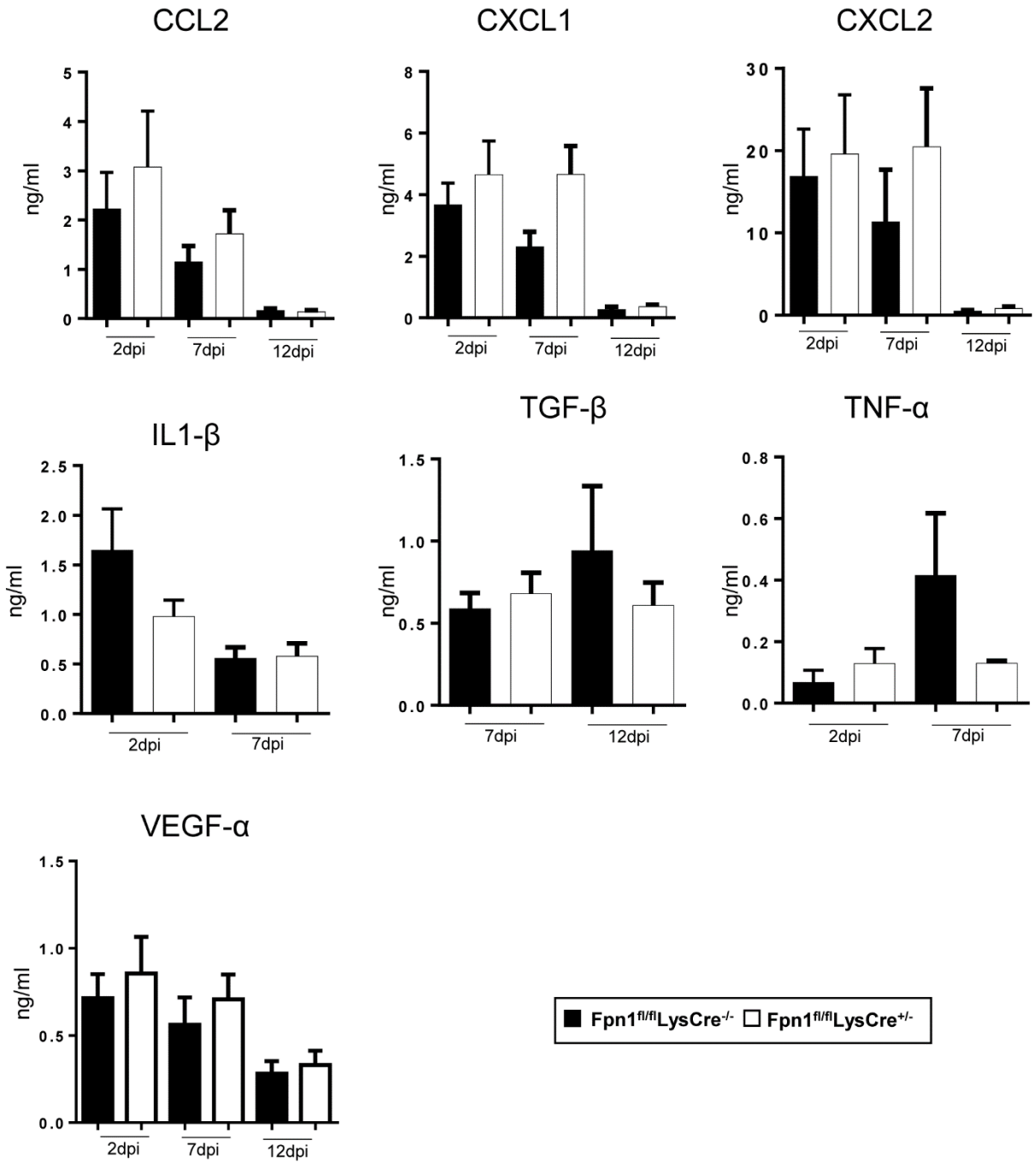

Figure S5. Cytokines and growth factors levels in skin wound are not altered in Fpn1$^{fl/fl}$LysCre$^{+/-}$ mice.

CCL2, CXCL1, CXCL2, IL-1□, TGF□, TNF□ and VEGF□□protein levels in wound lysates were assessed by ELISA at different times after skin injury. At the time points not shown, the levels of the respective cytokine were below the detection limit of the assay. The histograms show the mean ± SEM. n = 10 mice for each group.